



New evidence for millennial-scale interactions between Hg cycling and hydroclimate from Lake Bosumtwi, Ghana

Alice R. Paine^{1*}, Joost Frieling¹, Timothy M. Shanahan², Tamsin A. Mather¹, Nicholas McKay³, Stuart A. Robinson¹, David M. Pyle¹, Isabel M. Fendley¹, Ruth Kiely⁴, William D. Gosling⁴

¹Department of Earth Sciences, University of Oxford, UK, OX1 3AN

²Department of Earth and Planetary Sciences, University of Texas at Austin, Texas, USA

³School of Earth and Sustainability, Northern Arizona University, Flagstaff, Arizona, USA

⁴Institute for Biodiversity & Ecosystem Dynamics, University of Amsterdam, Amsterdam, Netherlands

*Corresponding Author: alice.paine@earth.ox.ac.uk

Changing hydrology impacts the biogeochemical cycling of elements such as mercury (Hg), whose transport and transformation in the environment appear linked to hydroclimate on diverse timescales. Key questions remain about how these processes manifest over different timescales and their potential environmental consequences. For example, millennial-scale Hg-hydroclimate interactions in the terrestrial realm are poorly understood, as few sedimentary records have sufficient length and/or resolution to record abrupt and long-lasting changes in Hg cycling, and the relative roles of depositional processes on these changes. Here, we present a high-resolution sedimentary Hg record from tropical Lake Bosumtwi (Ghana, West Africa) since ~96 ka. A coupled response is observed between Hg flux and shifts in sediment composition, the latter reflecting changes in lake level. Specifically, we find that the amplitude and frequency of Hg peaks increase as the lake level rises, suggesting that Hg burial was enhanced in response to an insolation-driven increase in precipitation at ~73 ka. A more transient, threefold increase in Hg concentration and accumulation rate is also recorded between ~13 and 4 ka, coinciding with a period of distinctly higher rainfall across North Africa known as the African Humid Period. Two mechanisms, likely working in tandem, could explain this correspondence: (1) an increase in wet deposition of Hg by precipitation and (2) efficient sequestration of organic-hosted Hg. Taken together, our results reaffirm that changes in hydroclimate, directly and/or indirectly, can be linked to millennial-scale changes in tropical Hg cycling, and that these signals can be recorded in lake sediments.

1. Introduction

Mercury (Hg) is a volatile and toxic metal released into the atmosphere as a result of natural processes (e.g., volcanism, geothermal activity, weathering; Edwards et al., 2021; Selin, 2009) and, more recently, human activities (e.g., industrial activities, mining, coal burning; Amos et al., 2015). Approximately 95 % of atmospheric Hg exists in gaseous elemental form (Hg⁰). An atmospheric



39 lifetime of up to 2 years permits its transport over long distances prior to removal by wet or dry
40 deposition, and following oxidation and aerosol scavenging (Lyman et al., 2020). Once free gaseous
41 (Hg^0) and/or oxidised (Hg^{II}) Hg has been deposited into the terrestrial environment, two sets of
42 reactions become particularly important: (1) oxidation-reduction, and (2) methylation-demethylation
43 (Branfireun et al., 2020). The reduction of Hg^{II} to Hg^0 can result in release back into the atmosphere.
44 Hg^{II} can also be bound to organic matter (OM) or sulphides, and thus be sequestered and
45 accumulated in sediments (Åkerblom et al., 2013; Hsu-Kim et al., 2013; Mason et al., 2000).
46 Accumulation of Hg in the terrestrial environment is therefore a function of the balance between Hg
47 removal from and re-emission to the atmosphere, and governed by the rate and intensity of different
48 thermal, photo, and biogenic reactions (Bishop et al., 2020; Obrist et al., 2018).

49 The exchange of Hg between the terrestrial biosphere, hydrosphere, critical zone, and atmosphere
50 are intrinsically coupled to climate. Changes in ecosystem Hg loading, overland transport, and
51 methylation have all been directly linked to decadal-scale changes in global temperature and
52 precipitation, and their associated shifts in terrestrial productivity, land-atmosphere exchange, and
53 wildfire dynamics (Bishop et al., 2020; Li et al., 2020). However, studying the long-term natural Hg
54 cycle presents several challenges. For example, the overwhelming increase in anthropogenic Hg
55 fluxes in recent decades have substantially altered the environmental dynamics of this cycle,
56 complicating assessment of how long-term climate change may alter its rate, intensity, and evolution
57 (United Nations Environment Programme, 2018). Pre-industrial-age archives allow for clear
58 comparison between natural and anthropogenic-driven changes in Hg cycling, and identification of
59 which regions may be most vulnerable to the negative effects of these changes, and highlight the
60 importance of understanding the long-term Hg cycle (e.g., Cooke et al., 2020; Segato et al., 2023).

61

62 **1.1 Mercury cycling and hydroclimate.**

63 The transport and transformation of Hg at the Earth's surface is directly linked to the hydrological
64 cycle (Bishop et al., 2020; Selin, 2009). Water plays a direct role in the efficiency of both Hg
65 deposition and re-emission. For example, changes in precipitation patterns can influence the
66 proportion of Hg removed from the atmosphere by wet versus dry deposition, with higher precipitation
67 amounts generally corresponding to enhanced Hg deposition at the surface (Amos et al., 2015;
68 Guédron et al., 2018). Elevated Hg concentrations have been measured in equatorial ocean surface
69 waters corresponding to inter-annual peaks in precipitation, with general circulation model simulations
70 suggesting that these are likely due to higher net Hg flux by wet deposition (Kuss et al., 2011;
71 Soerensen et al., 2014; Sprovieri et al., 2010). Multi-year monitoring by the Global Mercury
72 Observation System (GMOS) has similarly revealed distinct interannual differences in total wet
73 deposition of Hg, with the highest fluxes typically occurring in the wettest years (Leiva González et al.,
74 2022; Sprovieri et al., 2017). Precipitation also facilitates Hg transport in terrestrial watersheds, with
75 simultaneous increases in river discharge, surface runoff, and soil erosion during and after intense
76 storm events all enhancing hydrological 'connectivity' between surface environments and feeder



77 tributaries (Bishop et al., 2020). This enhances overland transport of Hg and other suspended
78 materials, and subsequently their delivery to lake and near-shore marine sediments (Liu et al., 2021;
79 Zaferani and Biester, 2021).

80 Water also plays an indirect role in drawdown and sequestration of Hg in aquatic environments.
81 Systems that are particularly sensitive to changes in water balance (e.g., terrestrial lakes) are most
82 likely to experience distinct, hydro-climate driven environmental changes that impact their internal Hg
83 cycle (Branfireun et al., 2020). For example, changes in organic matter cycling between the
84 catchment and the lake (Ravichandran, 2004), algal scavenging (Outridge et al., 2019), and early
85 diagenesis (Frieling et al., 2023). A decline in the total water volume of a basin may also elicit a
86 reduction in stratification (Woolway et al., 2020), during which increased mixing would ventilate
87 bottom waters and reduce organic-matter burial (Gulati et al., 2017). Conversely, a simultaneous
88 increase in total water volume and nutrient influx may increase stratification and bottom-water anoxia
89 to such an extent, that the system experiences a distinct increase in organic matter burial (Pilla et al.,
90 2020). Studies have also found catchment and basin structure to be important when considering the
91 extent to which sedimentary Hg signals reflect hydroclimate-driven variability, as both influence the
92 ease with which water is able to transport Hg to, from, and between discrete terrestrial sinks (Paine et
93 al., 2024).

94 Earth's hydroclimate is highly variable in space and time (Bradley and Diaz, 2021). In the short-term,
95 these interactions may manifest as annual changes in rainfall intensity and seasonality, or by sub-
96 decadal fluctuations in regional-scale climate modes (e.g., El-Nino Southern Oscillation, North Atlantic
97 Oscillation; Hernández et al., 2020). In the long-term, variability in the form of prolonged droughts
98 and/or pluvials may occur in response to global-scale atmospheric reorganization lasting centuries,
99 and changes in the planet's orbital configuration on timescales of many millennia (Bradley and Diaz,
100 2021). These wet-dry oscillations are important on a continental-scale. For example, periods of
101 extreme hydroclimate variability are known to have caused major changes in environmental
102 conditions across sub-Saharan Africa during the late Pleistocene, lasting for multiple millennia (e.g.,
103 Scholz et al., 2007).

104 Millennial-scale changes in hydroclimate may also affect the Hg cycle. Sediment cores extracted from
105 the Pacific and Atlantic oceans show low-amplitude Hg signals corresponding to orbital-scale ($>10^4$ -
106 year) changes in precipitation and rates of sediment delivery to the ocean (e.g., Chede et al., 2022;
107 Fadina et al., 2019; Figueiredo et al., 2022; Zou et al., 2021), and a growing number of terrestrial
108 successions also show Hg fluctuations coeval with climate-driven changes in local precipitation, cloud
109 formation, and ice/permafrost extent (e.g., Guédrón et al., 2018; Nalbant et al., 2023; Paine et al.,
110 2024; Pan et al., 2020; Pérez-Rodríguez et al., 2018). However, few terrestrial Hg records extend
111 beyond the present interglacial (>12 ka), and even fewer come from the low-latitudes: where tropical
112 rainforest, grassland and desert biomes are highly sensitive to millennial-scale hydroclimate variability
113 (Bradley and Diaz, 2021; Schneider et al., 2023). Thus, our current understanding of Hg behaviour
114 may not fully account for the impact of major, long-term hydroclimate changes on Hg transformation



115 and transport through tropical environments (Obrist et al., 2018; Schneider et al., 2023), highlighting
116 the need for new Hg records spanning long (>10³-year) timescales.

117

118 **1.3 West African Monsoon**

119 Sedimentary records offer an opportunity to assess the impact of millennial-scale hydroclimate
120 variability, and related effects, on the terrestrial Hg cycle. In its domain, the West African Monsoon
121 (WAM) regulates precipitation amount and distribution, and drives long-term evolution of
122 environmental characteristics and mineral-dust emissions (Kaboth-Bahr et al., 2021; Weldeab et al.,
123 2007). Proxy records from sub-Saharan Africa show that orbitally-driven variations in the strength of
124 the WAM have frequently driven severe drought events (Cohen et al., 2007; Scholz et al., 2007) and
125 humid periods (Armstrong et al., 2023; Menviel et al., 2021) throughout the Pleistocene. These humid
126 and arid periods have been linked to distinct changes in vegetation structure, ecosystem dynamics,
127 and human evolution across the continent (e.g., Cohen et al., 2022; Foerster et al., 2022; Gosling et
128 al., 2022b). This study focusses on sediment core BOS04-5B extracted from Lake Bosumtwi, Ghana
129 (West Africa), which provides a clear and continuous record of this hydroclimate variability (Koeberl et
130 al., 2007).

131 Lake Bosumtwi is a closed system isolated from the regional groundwater network, rendering it
132 sensitive to both short and long-term variability in rainfall, humidity, and dynamic surface processes
133 (Shanahan et al., 2008b; Turner et al., 1996). Integrated proxy data shows that Lake Bosumtwi
134 experienced dramatic changes in water balance, aeolian dust inputs, and biological productivity
135 throughout its history. These changes all correspond to moisture-driven oscillations between a forest
136 and grass-dominated catchment in response to insolation-driven variability in WAM strength, and
137 migration of the Intertropical Convergence Zone (ITCZ) (Gosling et al., 2022a; Miller et al., 2016; Peck
138 et al., 2004). Focussing on the uppermost ~47 m of the Lake Bosumtwi sediment record, this study
139 aims to assess whether major shifts in local hydroclimate produced measurable changes in how Hg
140 has been transported to, and buried within, this system since ~96 ka. By comparing our sedimentary
141 Hg record with proxy data from archives across the African continent (e.g., Foerster et al., 2022;
142 Scholz et al., 2007), we explore whether hydroclimate has exerted a measurable effect on terrestrial
143 Hg cycling in the WAM domain in over the past ~100-kyr.

144

145 **2. Site Description**

146 **2.1. Lake Bosumtwi**

147 Lake Bosumtwi is the only natural lake in Ghana, West Africa (6°30' N, 1°25' W) (**Fig. 1**). It occupies a
148 1.08 ± 0.04 Ma meteorite impact crater (Jourdan et al., 2009), excavated in metamorphosed and
149 crystalline rocks of the Birimian Supergroup (~2 Ga). The present-day lake is ~8.5 km in diameter,
150 with a water depth of up to 80 m at the lake centre, and the lake water level is currently at least 120 m



151 below the crater rim (Shanahan et al., 2007). The crater itself is ~10.5 km in diameter at the rim with
152 steep slopes, and a well-defined spillway (~120 m above the present lake surface) marks evidence of
153 lake overflow likely during the most recent humid period (**Fig. 1**) (Shanahan et al., 2015). The lake is
154 meromictic, with a shallow oxycline located ~10–15 m below the water's surface (Turner et al., 1996).

155 The Bosumtwi basin is hydrologically closed with no external drainages, connection to the regional
156 groundwater aquifer, river or stream inflow originating outside of the crater (**Fig. 1**) (Turner et al.,
157 1996). Only during exceptionally high lake levels does water leave the lake, through the spillway
158 (Shanahan et al., 2007). Approximately 300 m of sediment has accumulated in the centre of the basin
159 originating from biological processes within the lake, progressive erosion of the crater wall, aeolian
160 transport, and vegetation within the crater (Koeberl et al., 2005).

161

162 **2.1.1. West African Climate**

163 Seasonal variability in the tropical rain belt position drives short-term (<10-year) hydroclimate change
164 in West Africa. During boreal summer, an increase in northern hemisphere summer (June to August)
165 insolation triggers a northward ITCZ shift, creating a pressure gradient that brings moisture eastwards
166 from the Atlantic Ocean to western Africa. The opposite occurs in boreal winter (December to
167 February), where the ITCZ is displaced southwards, bringing dry, aerosol-rich, continental trade winds
168 to West Africa. Together, these seasonal shifts produce distinct annual wet (May to October) and dry
169 seasons.

170 On longer (>10⁴-year) timescales, hydroclimate variability in West Africa has been linked to cyclic
171 changes in Earth's orbital configuration. Changes in axial precession produce fluctuations in seasonal
172 insolation above the African continent, influencing the strength of the WAM, the Walker Circulation,
173 the position of the ITCZ, and the availability of continental moisture (Gosling et al., 2022b; Kaboth-
174 Bahr et al., 2021; Trauth et al., 2021). High precession causes weakening of the WAM and southward
175 migration of the ITCZ, producing drier conditions in West Africa and subsequent reductions in
176 terrestrial precipitation, ecosystem productivity, and recession of terrestrial forests (Menviel et al.,
177 2021). Conversely, strengthening of the WAM and a more northerly ITCZ position is documented
178 when precession is low, bringing wetter and warmer conditions to West Africa and causing expansion
179 of dense forests, voluminous lakes, and diverse ecosystems (Larrasoña et al., 2013; Pausata et al.,
180 2020).

181

182 **2.1.2. Local hydrology and vegetation**

183 Approximately 49% of the Bosumtwi drainage basin (area: 106 km²) is currently occupied by the lake.
184 Situated in close proximity to the (current) ecological transition-zone between savannah in the north
185 and moist forest in the south, Lake Bosumtwi lies directly in the seasonal migration path of the ITCZ
186 (Nicholson, 2013). It experiences a current mean annual temperature of ~26°C, ranging between
187 ~23°C in August to ~27°C in February, with cooler summer temperatures attributed to increased



188 cloudiness and related reduction in incoming solar radiation (Shanahan et al., 2007). Present-day
189 humidity ranges from ~85% in August to ~75% in January, and average annual precipitation is ~1450
190 mm (Turner et al., 1996). At present, the surrounding catchment as classified as a 'Tropical and
191 Subtropical Moist Broadleaf Forest' biome (White, 1983), meaning it is heavily forested with well-
192 developed tropical soils, although many flat-lying areas have been converted to agriculture (e.g.,
193 maize, plantain, cocoa, and oil palm) in recent decades (Boamah and Koeberl, 2007). Before human
194 occupation of the site, the lake was surrounded by a moist semideciduous forest, with a canopy
195 including abundant of trees from the Ulmaceae and Sterculiaceae (flowering plant) families (Miller and
196 Gosling, 2014).

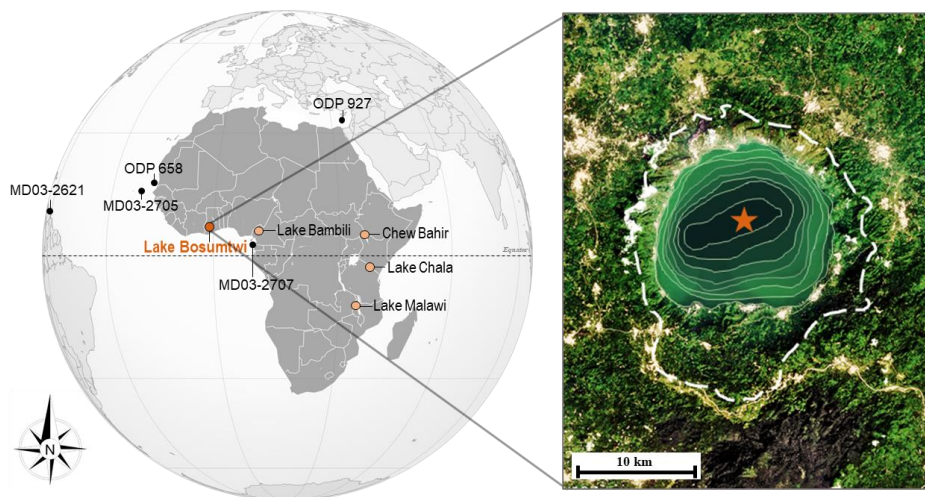


Figure 1: (Left) Location of key lake and marine sediment archives in and around Sub-Saharan Africa (SSA). (Right) An aerial photograph of Lake Bosumtwi (copyright: NASA, 2018), on which the location of the BOS04-5B drill site is marked as an orange star. Contours show lake bathymetry, with each step representing a 10 m depth change and culminating in a maximum depth of 75 m (Shanahan et al., 2012). The spillway notch is in the eastern rim of the crater, and the dashed white line marks the extent of the drainage divide (Brooks et al., 2005; Shanahan et al., 2006).

197

198 2.1.3. Paleoclimatic significance

199 Lake Bosumtwi provides an excellent record of millennial-scale hydroclimate change in West Africa.
200 The upper ~47 m of sediment corresponds to the interval ~96 ka to present, and contains a series of
201 distinct lithological features suggesting pronounced, climate-driven changes in lake level, catchment
202 structure, and sediment transport processes (Gosling et al., 2022a; McKay, 2012; Miller et al., 2016).
203 For example, a massive, clastic-rich blue-grey clay unit is present between ~34 and 32 m depth,
204 where TOC values drop to <1% and bulk density values increase by >60% (Scholz et al., 2007).
205 Interpreted and referred to as Arid Interval(AI)-1 (McKay, 2012), this unit formed during extremely dry



206 climatic conditions leading to near-total desiccation of the lake, and this interpretation is further
207 supported by identification of a clear erosional unconformity corresponding to the age of the AI-1 unit
208 in seismic reflection profiles (Brooks et al., 2005; Scholz et al., 2007).

209 Changing physical properties and geochemistry of sediments deposited prior to and following Unit AI-
210 1 appear to reflect regional hydroclimate shifts (Scholz et al., 2007). Prior to AI-1, the presence of
211 clastic-rich, organic-depleted sediments suggest a progressive reduction in water depth, likely in
212 response to a (long-term) negative water balance (McKay, 2012; Shanahan et al., 2008b). Following
213 AI-1, an abrupt reduction in clastic material concentrations, increased TOC, diagenetic carbonate, and
214 lamination frequency all imply oxygen depletion at the sediment-water interface – evidence for a shift
215 to a positive water balance (McKay, 2012; Scholz et al., 2007; Shanahan et al., 2008a). The core also
216 shows distinct co-enrichment in manganese (Mn) and iron (Fe) in certain intervals following AI-1,
217 which are associated with manganosiderite (Mn-rich FeCO_3) precipitation in the lake sediments.
218 Manganosiderite requires anoxic non-sulphidic (ferruginous) pore-water conditions and high dissolved
219 inorganic carbon concentrations to precipitate (Brumsack, 2006; Tribouillard et al., 2006), and
220 appears as a consequence of the redox tower migrating into the water column: a response to
221 increasing water column stratification, and overall lake level (Shanahan et al., 2006). The closed
222 hydrology of Lake Bosumtwi means that changing water levels are likely to reflect the magnitude of
223 precipitation variability in the region, with higher lake levels typically occurring during wetter climate
224 intervals (Russell et al., 2003; Shanahan et al., 2008b).

225

226 **3. Material and methods**

227 **3.1. BOS04-5B**

228 Core BOS04-5B was recovered in 2004 as part of the International Continental Drilling Program
229 (Koeberl et al., 2005) (full details in **S1**). Our study focuses on the upper ~47 m section of a 296-m-
230 long core extracted from deep-water (76 m) site 5 (core BOS04-5B), which extends from the present-
231 day lake floor to the brecciated bedrock dated by $^{40}\text{Ar}/^{39}\text{Ar}$ to 1.08 ± 0.04 Ma (Jourdan et al., 2009).
232 Over ~67% of the full 294 m-long (~1-Myr) sediment succession is laminated (Koeberl et al., 2007),
233 with distinctive alternating clastic, organic and carbonate laminae (Shanahan et al., 2012, 2009,
234 2008a). Thicker laminations are visible either as packets of light grey microturbidites, or distinct yellow
235 and orange carbonates produced by enhanced redox-related precipitation of Fe and Mn bearing
236 minerals (Shanahan et al., 2008a).

237

238 **3.2. Chronology**

239 Age control for the ~47 m of sediment analysed in this study is provided by the BOSMORE7 model,
240 generated by Gosling et al. (2022). Using a combination of radiocarbon (calibrated ^{14}C ; $n=109$),
241 optically stimulated luminescence (OSL; $n=22$) and uranium-thorium (U/Th; $n=5$) dates as



242 independent tie-points, Bayesian modelling suggests that the upper ~47 m of sedimentation at Lake
243 Bosumtwi corresponds to the interval ~96–0 ka (full details in **S3**) (Gosling et al., 2022a; Shanahan et
244 al., 2013). Age estimates for the AI-1 sedimentary unit are constrained by ¹⁴C, OSL and U-Th dating
245 of the surrounding sediments, and suggest this unit formed between 77 and 71 (±5) ka (Scholz et al.,
246 2007; Shanahan et al., 2008b). The duration of the event is less clear due to the excessive erosion of
247 the newly exposed crater walls and reduction in distance between the shore and 5B core site (McKay,
248 2012) which may have led to unusually high sedimentation rates during this interval. Thus, slight
249 underestimation of sediment ages immediately following unit AI-1 may be expected.

250

251 **3.3. Sediment geochemistry**

252 **3.3.1. Mercury**

253 Total Hg (Hgr) in the bulk sediments of core BOS04-5B was measured using the RA-915 Portable
254 Mercury Analyzer with PYRO-915+ Pyrolyzer, Lumex (Bin et al., 2001) at the University of Oxford. For
255 this study, we analysed 165 samples spanning the composite depth interval 47.7 to 0 m, with an
256 average temporal resolution of ~0.6 ka between each sample. Dry powdered sample material (45–
257 100 mg) was heated to ~700°C, volatilizing Hg in the sample. Atomic absorption spectrometry of the
258 gases produced during pyrolysis quantifies the total Hg content of the sample. Six different quantities
259 of standard material (paint-contaminated soil – NIST Standard Reference Material ® 2587) with a
260 known Hg value of 290 ± 9 ng g⁻¹ were run to calibrate the instrument before sample analysis, and
261 then one standard for every 10 lacustrine samples. Calibration results accompany this article in a
262 supplementary dataset. Long-term observations of standard measurements (*n* = 390) for this
263 instrument show average reproducibility (1 sigma) of 6% for samples with ≥10 ng g⁻¹ Hg (Frieling et al.
264 2023). Four (2%) of the analysed samples contained very low Hg contents (<10 ng g⁻¹), and likely
265 have uncertainties ≥10 %. Details of standard runs are included as a supplementary file.

266

267 **3.3.2. Organic and inorganic carbon**

268 Quantitative values for total organic carbon (TOC) and total inorganic carbon (TIC) content were
269 measured on the same powdered sample material also analysed for Hg, using a Strohlein Coulomat
270 702 (Jenkyns and Weedon, 2013) at the University of Oxford. Analytical reproducibility for this
271 instrument was ≤0.2 % based on repeat measurements, with a detection limit of ca. 0.1–0.2 %.

272 Powdered BOS04-5B sediment samples were split into two aliquots. Weights for aliquot 1 were
273 between 50–70 mg, and aliquot 2 between 90–120 mg. Prior to coulometric analysis, aliquot 2
274 samples were furnace for 24 hours at 420°C in order to remove organic carbon fractions. Both
275 aliquots were then combusted in oxygen at 1220°C to break down the calcium carbonate and produce
276 carbon dioxide (CO₂), which was fed into a solution of barium perchlorate. By producing a change in
277 solution pH from an initial value of 10.0, back titration to the original pH using electrolysis provided a
278 measure of the amount of carbon originally present – quantified by the amount of electricity required



279 to restore a pH of 10.0 and recorded in counts (Jenkyns, 1988; Jenkyns and Weedon, 2013). Counts
280 obtained for aliquots 1 and 2 were used to calculate the total carbon (TC) content of each aliquot in
281 wt.%, using the formula:

$$282 \quad TC = \frac{\text{total counts} \times 0.2}{M} \quad (\text{eqn. 1})$$

283 where M is the sample mass in mg.

284 TOC was calculated as follows:

$$285 \quad TOC = TC_1 - TC_2 \quad (\text{eqn. 2})$$

286 where TC_1 and TC_2 represent the TC values obtained for aliquots (1) and (2), respectively. TC_2
287 represents the TIC value for the sample.

288

289 **3.3.3. Authigenic carbonates**

290 The BOS04-5B succession contains variable amounts of diagenetic carbonates, predominantly
291 (mangano-)siderite (**Fig. S2**) (McKay, 2012). Siderites commonly form in freshwater settings at
292 shallow sediment depths under anaerobic (anoxic) conditions accompanied by organic-rich sediments
293 (Armenteros, 2010; Sebag et al., 2018). However, they can also preclude accurate measurement of
294 organic carbon content in lacustrine sediment via pyrolysis- or furnace-based methods, causing
295 systematic overestimation of total organic carbon (TOC) due to the fact that thermal decomposition of
296 siderite typically starts at temperatures $<420^\circ\text{C}$ (Sebag et al., 2018), which is lower than that which is
297 used to remove the organic fraction on the Coulomat (Jenkyns, 1988). To assess whether siderite-
298 associated carbon had an appreciable impact on the TOC measurements, we also analysed the
299 carbon release from sixteen BOS04-5B samples spanning a range of low to high XRF-derived Mn
300 counts (i.e., covering the possible range of (mangano-)siderite contents) using a weak acid (warm 5%
301 HCl) treatment, following established methodologies (Brodie et al., 2011; Vinduřková et al., 2019).
302 Full details are provided in **S6**. Comparison of acid-treated and furnaced samples showed no
303 systematic offset nor a clear correlation with the Mn counts from XRF data (**Fig. S2c**), suggesting that
304 the carbon release from siderite did not appreciably bias TOC measurements.

305

306 **3.3.4. Scanning X-Ray fluorescence**

307 The Hg data for core BOS04-5B generated in this study are paired with unpublished x-ray
308 fluorescence (XRF) data (McKay, 2012). The bulk elemental composition of the core was quantified
309 using the Itrax® scanning XRF analyser at the Large Lake Observatory at the University of
310 Minnesota. Core material was analysed at 1-cm-resolution with 60 sec count times, and a Mo X-ray
311 source run at 30 kV and 20 mA. Analytical and correctional procedures for element abundance
312 measurements covering the upper ~159 m (~500-kyr) of BOS04-5B are fully described in **S7**.



313

314 **3.4. Mercury normalization**

315 It is common practice to assess both total Hg concentration (Hg_T) and normalised Hg (Hg/X) with the
316 aim to reduce, at least partially, the potential impact of variability in a dominant carrier/host phase (X)
317 on Hg_T (Sanei et al., 2012; Shen et al., 2020). Organic matter (here expressed as TOC) is commonly
318 considered the primary host phase of sedimentary Hg (Ravichandran, 2004). However, variability in
319 Hg_T may also be associated with variability in the abundance of detrital minerals, usually detected by
320 a correlation between Hg and detrital elements such as Al or K (Paine et al., 2024; Them et al., 2019),
321 and very rarely in sulphate-limited (lacustrine) sediments, sulphides (Benoit et al., 1999; Han et al.,
322 2008). Exploration of Hg signal variability relative to distinct shifts in the abundance, contribution
323 and/or sources of host phases can therefore elucidate the timing and magnitude of shifts in lake
324 hydrology, sedimentation regime, and geochemistry, and whether these are connected to changes in
325 the Hg cycle or sediment composition changes (Paine et al., 2024).

326 To isolate the effects of local depositional and/or transport processes on Hg signals recorded in the
327 sediments of Lake Bosumtwi, we normalised Hg_T values to organic matter (TOC) and detrital mineral
328 abundance estimated from potassium (K) intensities; with the assumption that the strongest positive-
329 sloped linear correlation with Hg_T among these elements signals the most likely dominant impact of
330 host phase variability in that section of the core. To account for differences in resolution between Hg
331 and XRF data, K measurements were averaged to obtain a K value corresponding to the interval
332 covered by each discrete Hg sample (~0.5 cm thickness).

333

334 **3.5. Mercury accumulation**

335 The total Hg mass accumulation rate (Hg_{AR}) in core BOS04-5B was calculated from:

$$336 \quad Hg_{AR} = Hg_T (DBD \times SR) \quad (eqn. 3)$$

337 where Hg_{AR} is in $mg\ m^{-2}\ kyr^{-1}$, Hg_T is the total mercury concentration ($mg\ g^{-1}$), DBD is the dry bulk
338 density ($g\ m^{-3}$), and SR is the sediment accumulation rate ($m\ kyr^{-1}$). Values for Hg_{AR} are also
339 calculated with respect to the median age estimate for each sample. We do not present maximum
340 and minimum Hg_{AR} values here, but note that uncertainties increase with depth due to increasing
341 uncertainties in sedimentation rates, which are calculated based on the BOSMORE7 age model and
342 average $-0.08\ cm\ yr^{-1}$ ($0.02-0.3\ cm\ yr^{-1}$).

343 DBD values were calculated using measurements obtained by loss-on-ignition (McKay, 2012;
344 Shanahan et al., 2013), using the formula:

$$345 \quad DBD = M_{solid}/V_{total} \quad (eqn. 4)$$



346 where M_{solid} is the mass of dry solid material (g) in each sample, and V_{total} is the volume of each
347 respective sample (0.5 cm^3). To calculate M_{solid} , the proportion of clastic material was multiplied by an
348 assumed grain density value (2.6 g cm^{-3}) representative of a mixture of common sedimentary
349 minerals (e.g. quartz, clay minerals, clastic; typically range of 2.6 to 3 g cm^{-3}) and the total volume.
350 The proportion of clastic material was calculated by first accounting for the proportion of water and
351 organic matter (measured by McKay (2012) and Shanahan et al. (2013) in each sample and
352 assuming the residual was all clastic material. DBD values generally increase with core depth, which
353 reflects the impact of increasing sediment compaction and dewatering with age (Shanahan et al.,
354 2013). Calculated values of DBD average 1.15 g cm^{-3} , which is broadly consistent with measurements
355 taken from other African lake sediment successions of similar age ($<100 \text{ ka}$), composition (silty clays
356 between 0.6 – 1.1 g cm^{-3}), and structure (high porosity) (e.g., Cohen et al., 2016; Scholz et al., 2007).

357

358 4. Results

359 Core BOS04-5B from Lake Bosumtwi shows distinct fluctuations in total sedimentary Hg
360 concentration (Hg_T) throughout the $\sim 47 \text{ m}$ succession. Values range from 10 to 370 ng g^{-1} (median:
361 58 ng g^{-1}) (**Fig. 2**). The Hg_T curve broadly tracks that of TOC, which shows similarly pronounced
362 variability ranging between 0.1 to 23 wt. \% (median: 6.5 wt. \%) (**Fig. 2**), and peaking between 5.2 and
363 3 m depth. Calculated Hg accumulation rates (Hg_{AR}) do not follow the same pattern as Hg_T and TOC.
364 Ranging between 2.9 and $460 \text{ mg m}^{-2} \text{ kyr}^{-1}$, calculated values instead broadly track the sedimentation
365 rate curve presented in **Figure 2**. Large peaks in Hg_{AR} are visible between 8 and 6 m depth and then
366 again between 2 and 0 m , and these Hg_{AR} peaks are both coeval with reductions in TOC below ~ 10
367 wt. \% . The lowest Hg_{AR} values are recorded in the lower core section between ~ 47 and 34 m depth.

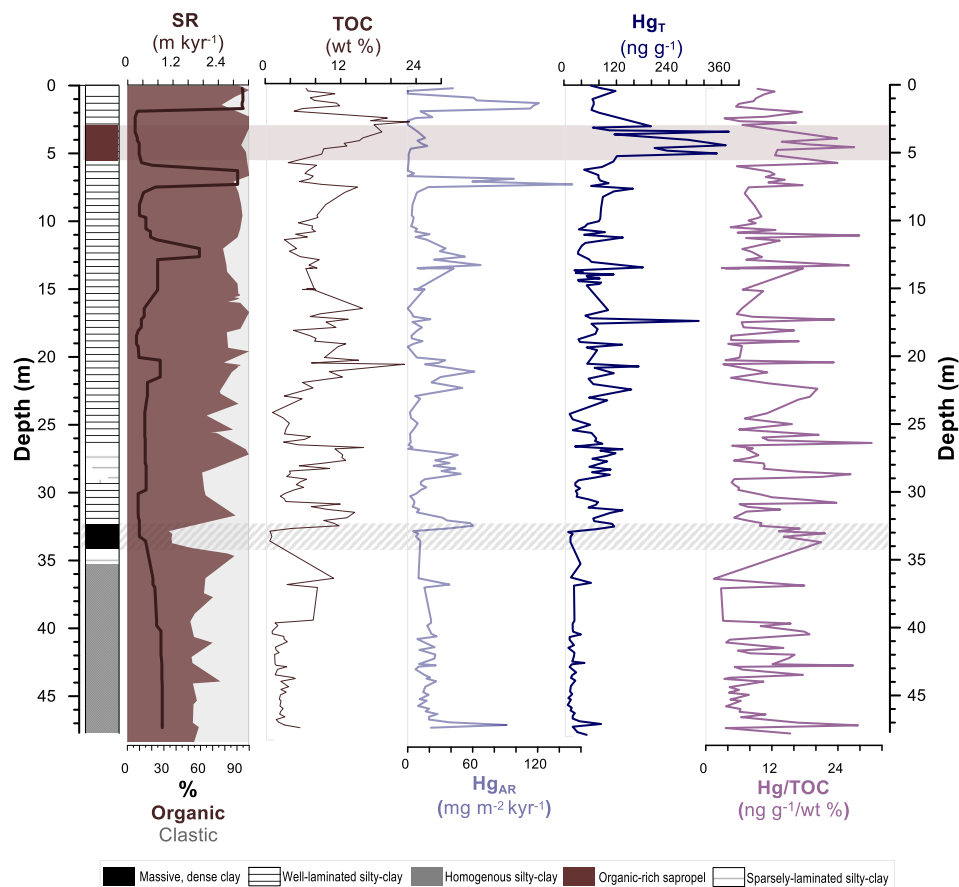


Figure 2: Depth-resolved profiles of total organic carbon (TOC), total Hg (Hg_T) and Hg accumulation rate (Hg_{AR}) profiles obtained for core BOS04-5B from Lake Bosumtwi in this study, relative to key lithofacies and sedimentological data including records of sedimentation rate (SR; *this study*), and the proportion of biogenic to terrigenous material (% organic) within the core (McKay, 2012). A distinct lake low stand referred to as Arid Interval 1 (AI-1) based on seismic profiles and sedimentological data is marked between 33.5 and 32.8 m depth (grey dashed shading; McKay, 2012; Scholz et al., 2007). Limited samples were available between ~39 and 34 m depth (Fig. S1). Sapropel layer Unit S1 is marked between 3–5.5 m depth (brown shading; Russell et al., 2003; Shanahan et al., 2008a; Talbot and Johannessen, 1992). We also present ratios of Hg_T to TOC, following evidence for a positive correlation between the two compounds ($r^2 = 0.42$) (see section 5.1).

368

369 Changing Hg signals in Lake Bosumtwi correspond to measurable changes in lake sedimentation.

370 From ~47 to 32 m depth, low amplitude, muted variability in both Hg_T and Hg_{AR} corresponds to a

371 homogeneous sequence of silty-clay sized material generally depleted in TOC, S, and high in detrital

372 materials. No clear changes in Hg_T nor Hg_{AR} are visible during AI-1 (34 – 32 m core depth), however,

373 variability in Hg concentration increases immediately following this interval. From ~32 m to the core



374 top, sediments show a progressive increase in Hg_T punctuated by several clear peaks, and more
375 pronounced fluctuations in Hg_{AR} (**Fig. 2**). This shift in Hg behaviour tracks a broad increase in the
376 organic content of the core compared to clastic, reflected by increasing TOC and decreasing K
377 profiles (**Fig. 2**). The clearest expression of this correspondence is seen between 5.2 and 3 m,
378 whereby the highest Hg_T values correspond to the organic-rich sapropel Unit S1.

379

380 5. Discussion

381 Studying time-resolved changes in lake sediment Hg concentration provides a valuable opportunity to
382 study changes in the pre-industrial Hg cycle, how these changes translate to measurable sedimentary
383 signals, and their links to local and regional-scale environmental variability (Cooke et al., 2020). From
384 the data presented in **Figure 2**, two mechanisms emerge as plausible drivers of Hg variability in Lake
385 Bosumtwi. First is external changes in net Hg input to the system, and second is organic matter (host)
386 availability. Both are explored in the discussion below.

387

388 5.1. Lacustrine host phases of mercury

389 An overall positive association between Hg_T and TOC ($r^2 = 0.42$) suggests that Hg variability may be
390 associated with organic carbon variability in Lake Bosumtwi. However, it is noteworthy that detrital
391 materials (e.g., K; $r^2 = 0.34$) show negative correlations with TOC and Hg (Fig. 3b) so that the Hg-
392 TOC correlation may reflect, in part, a correlation imposed by variable clay-dilution of both Hg and
393 TOC. The broad statistical link between Hg and TOC is supported by evidence for large Hg_T and Hg_{AR}
394 peaks in core sections containing high TOC concentrations, most markedly in the upper sections (**Fig.**
395 **2**), and the relationship between Hg_T and TOC also strengthens following deposition of Al-1 (**Fig. 3a,**
396 **S3**). However, the highest Hg_T values are not always recorded in the most TOC-enriched sediments,
397 nor are TOC-depleted sediments also depleted in Hg_T (**Fig. 2**). Dilution of Hg by organic matter is
398 unlikely to be the cause (Machado et al., 2016), nor can shift from an organic to detrital-dominated
399 host-phase regime account for these signals, given that intervals characterised by an overall negative
400 Hg and TOC correlation are coeval with similarly negative values for Hg and K (**Fig. S3**). More likely is
401 that they reflect changes in net Hg flux to the system, and hence the amount of Hg being supplied to
402 (and sequestered in) Lake Bosumtwi.

403 A negative overall correlation between Hg_T and K is apparent throughout the record ($r^2 = 0.34$; **Fig.**
404 **3a**). Other robust proxies for the proportion of detrital and autochthonous components in biogenic-rich
405 sediments include Fe, Ti, Rb, and Al (Grygar et al., 2019). Strong correlations between K and these
406 detrital elements confirm this is likely also the case in Lake Bosumtwi (**Fig. 3b**), with enrichment of
407 detrital materials in this core reflecting enhanced erosion and sediment transport to the BOS04-5B
408 drill site (McKay, 2012; Shanahan et al., 2012). Moreover, the significant negative correlations
409 between TOC, Hg_T , and all elements associated with detrital components (K, Ti, Rb, and Al) (**Fig. 3b**)



410 suggest that detrital matter did exert a control on Hg_T . However, instead of increasing Hg, the
 411 negative correlation with detrital material suggests that 'Hg-depleted' detrital materials diluted the
 412 concentration of both Hg and its suggested host (TOC). Variations in both the detrital and Hg flux may
 413 also explain the somewhat counterintuitive decoupling of Hg_T and Hg_{AR} in some intervals, for example,
 414 between ~10 and 6 m depth (**Fig. 2**). Dilution-driven alteration of the sedimentary Hg record may be a
 415 common feature for depositional systems where supply of Hg is ultimately limited by atmospheric
 416 inputs (e.g., Chede et al., 2022). Clear correlations between Hg_T and Mn, and Hg_T and Fe (redox
 417 sensitive elements) are also absent in this record (**Fig. S4**), suggesting that Hg concentrations in Lake
 418 Bosumtwi was not appreciably influenced by changes in redox conditions or diagenetic effects
 419 signalled by these elements.

420

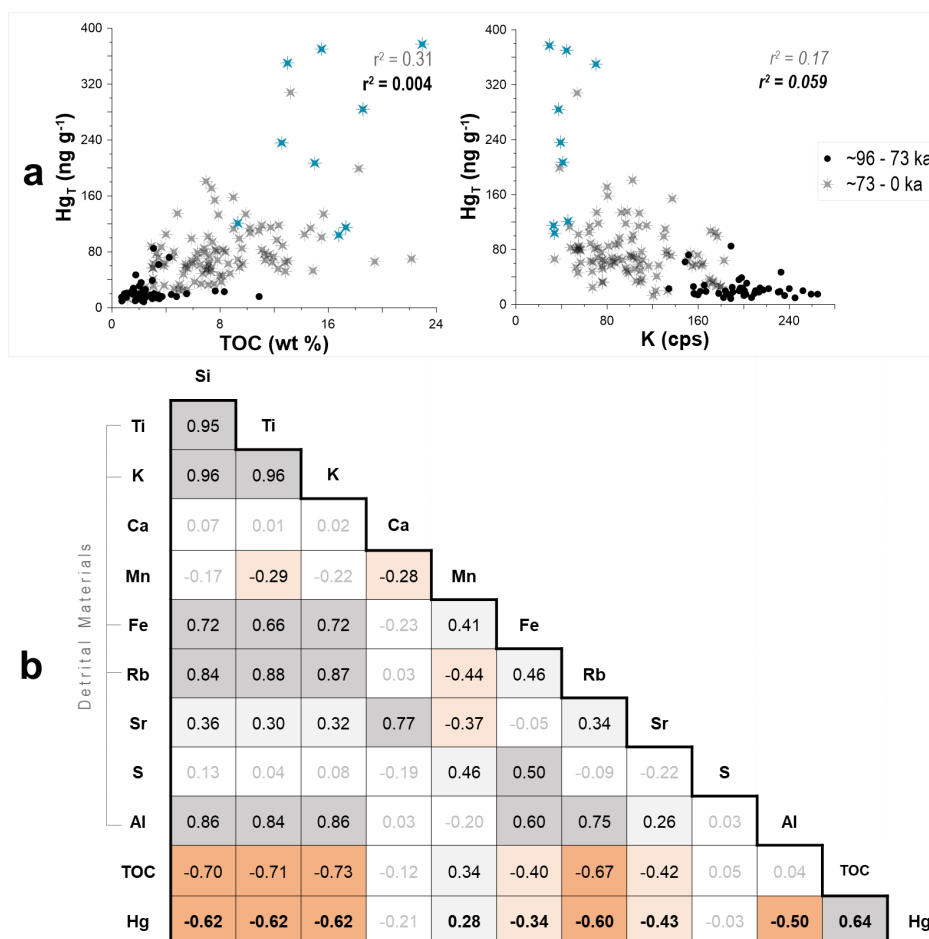


Figure 3: (a) Comparison of host-phase relationships in Lake Bosumtwi between ~96 and 73 ka (black circles), and between ~73 and 0 ka (stars). We assess the Hg_T record for this lake relative to total organic



carbon (TOC) values measured in this study, and detrital minerals (estimated by potassium (K)) concentrations measured by McKay (2012). R-squared (r^2) values for each interval are also given, with italic formatting indicating a negative relationship. Stars marked in teal correspond to deposition of sapropel unit 1 (S1) in BOS04-5B. **(b)** Full-core correlation (Pearson's r) matrix for Hg, total organic carbon (TOC) (this study), and a suite of trace elements measured in BOS04-5B by XRF (McKay, 2012). Higher r values suggest that similar processes influence the concentration of the two elements in focus. Grey shading marks positive correlations (light: >0.25 , dark: >0.5), and orange shading marks negative correlations (light: <-0.25 , dark: <-0.5). Unshaded boxes mark weak/negligible correlations (between 0 and 0.25, and 0 and -0.25), with values greyed-out for clarity. All remaining values are presented with black text, with those in this range related to Hg in the boldest type.

421

422 **5.2. Environmental drivers**

423 Time resolved Hg_T and Hg_{AR} profiles generated from the sediments of Lake Bosumtwi show two
424 broad periods of differing Hg behaviour: (1) $\sim 96 - 73$ ka (low Hg_T and Hg_{AR}) and (2) $\sim 73 - 0$ ka
425 (moderate/high Hg_T , and large fluctuations in Hg_T and Hg_{AR}) (**Fig. 4**). Each corresponds to different
426 lake level evolution trends with broadly decreasing lake level between ~ 96 and 73 ka (although with a
427 substantial rise between 95 and 80 ka), and rising from ~ 73 to 0 ka (**Fig. 4**). Lake Bosumtwi's
428 hydrology is controlled by a balance between direct precipitation and runoff with water removal limited
429 almost entirely to evaporation; exceptions being rare transient overspilling events (Turner et al.,
430 1996). Taking this unique hydrology into account, our discussion below explores how different
431 environmental processes relate to changes in Hg behaviour during these two discrete intervals, and
432 how the significance of these processes may have changed through time.

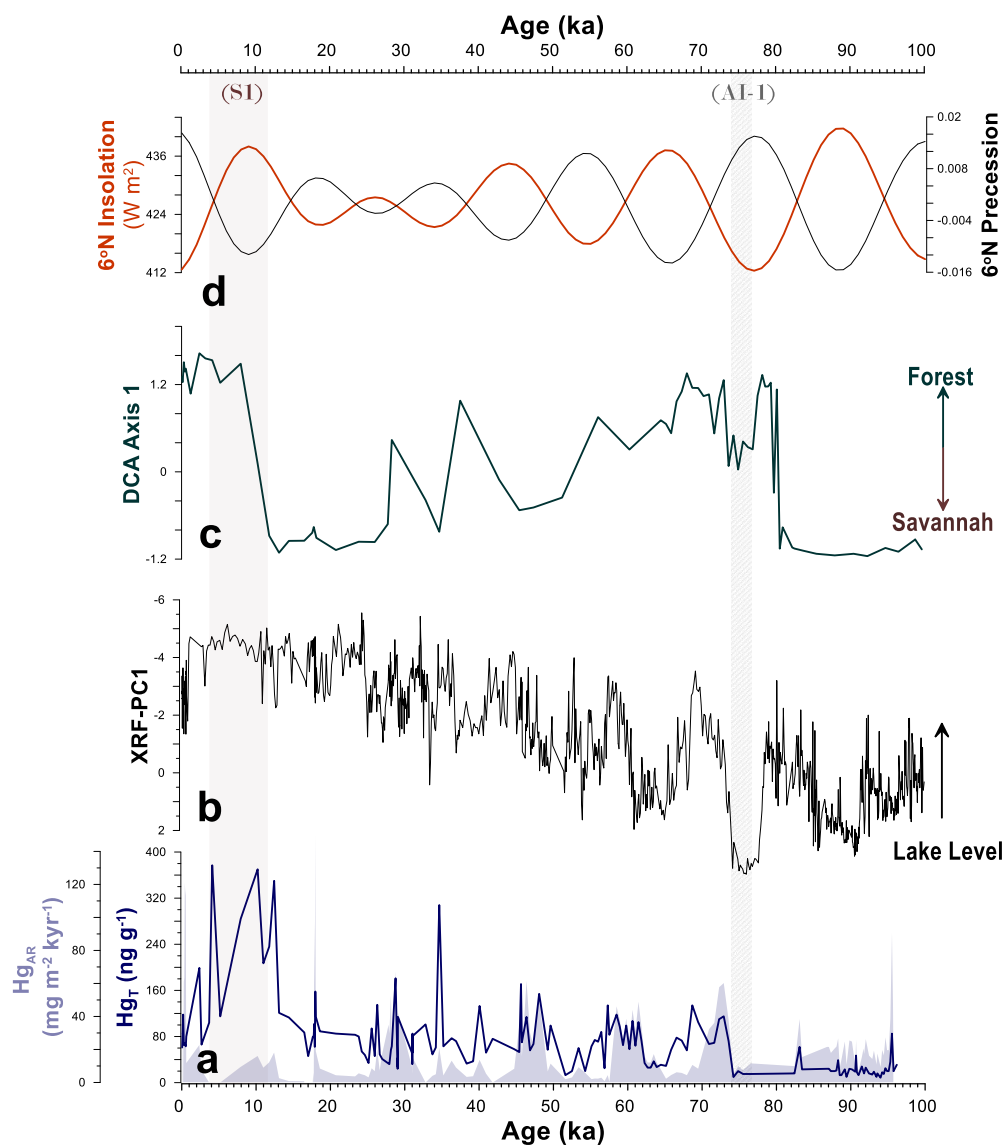


Figure 4: Comparison of key proxy datasets. **(a)** Total mercury (Hg_T) and mercury accumulation rate (Hg_{AR}) for Lake Bosumtwi from this study, chosen as the most appropriate proxies for Hg variability in this core (see **section 5.1**). **(b)** The first principal component (PC1) of the BOS04-5B XRF data (39% of total variance) is strongly associated with terrigenous elements, and so interpreted as an indicator of lake level changes (McKay, 2012). **(c)** Forest (woody) taxa abundance (presented as DCA Axis 1; Gosling et al., 2022a; Miller et al., 2016). Lack of data for woody taxa presence is assumed to imply a savannah-dominated regional landscape. **(d)** Annual mean insolation and precessional variability at 6°N latitude, calculated following the astronomical solution presented by Laskar et al. (2004) (accessed via. <https://vo.imcce.fr/insola/earth/online/earth/online/index.php>). Orbital precession



broadly induces millennial-scale (~19 to 23-kyr) fluctuations in insolation, and enhanced precessional amplitude has been linked to more severe hydroclimatic extremes in West Africa throughout the Pleistocene (Scholz et al., 2007). Proxy data are all presented on the BOSMORE7 chronology. Unit AI-1 is marked between 33.5 and 32.8 m depth (grey shading; Brooks et al., 2005; Scholz et al., 2007), and sapropel layer Unit S1 is marked between 3–5.5 m depth (brown shading; Shanahan et al., 2012, 2006).

433 5.2.1. ~96 to 73 ka

434 Both Hg_T and Hg_{AR} show muted variability between ~96 and 73 ka (**Fig. 4a**). The presence of more
435 clastic-rich/organic-depleted sediment (**Fig. 4b**), and reductions in tree pollen are both typical of a
436 savannah-dominant, more open landscape (**Fig. 4c**), and so suggest generally arid conditions within
437 the lake and its catchment prior to ~73 ka. These conditions would favour pronounced reductions in
438 lake level (McKay, 2012; Miller et al., 2016; Scholz et al., 2007), and are consistent with a 24 – 38%
439 reduction in local rainfall as estimated by water balance modelling) (Shanahan et al., 2008b).

440 Reductions in lake level could facilitate an increase in water column vertical mixing, ventilation of
441 bottom waters, more efficient breakdown of organic matter, and simultaneous sediment dilution by a
442 sudden increase in eroded material fluxes (McKay, 2012; Scholz et al., 2007; Shanahan et al., 2012)
443 – all of which could lead to a reduction in organic matter (host-phase) concentration. Indeed, several
444 meromictic lakes have shown reduced organic matter content as a function of better ventilation and
445 lower productivity during ‘shallow’ conditions (Katsev et al., 2010; Schultze et al., 2017), and new
446 evidence suggests that changes in organic matter oxidation may produce comparably distinct
447 changes in Hg sequestration (Tisserand et al., 2022).

448 The absence of a clear change in Hg_{AR} between ~96 and 73 ka might also reflect changes in the
449 balances of Hg cycling in the lake. Lake Bosumtwi is a hydrologically closed system that receives
450 >80% of its water from rainfall directly on the surface, meaning its hydrology and sedimentation
451 regime is extremely sensitive to variability in precipitation and precipitation-evaporation balance
452 (Shanahan et al., 2007; Turner et al., 1996). Thus, low Hg_T and Hg_{AR} values may reflect a reduction in
453 wet deposition of atmospheric Hg at the Lake Bosumtwi site by precipitation, while Hg evasion back to
454 the atmosphere remains high due to evaporation in the consistently warm, tropical temperatures
455 (Schneider et al., 2023). Depletion of sedimentary Hg during drier climate intervals are documented in
456 several other late Quaternary-age records, where they are interpreted as signs of a net reduction in
457 Hg input relative to loss/evasion (e.g., Hermanns and Biester, 2013; Pompeani et al., 2018; Schneider
458 et al., 2020; Schütze et al., 2021, 2018).

459 Desiccation of Lake Bosumtwi between ~75 and 73 ka (AI-1) corresponds to evidence for severe
460 depletion of organic matter, and enrichment of detrital materials within the sediments (**Fig. 2**).

461 Although a detailed characterization of local soil and bedrock Hg contents is currently lacking for Lake
462 Bosumtwi, these changes in sediment composition (lower TOC, higher K) and low overall
463 sedimentation rates are unaccompanied by coeval changes in Hg_{AR} (**Fig. 2**). In certain cases, one
464 would typically expect that the near-complete desiccation of a steep-sided lake would ‘focus’ trace



465 metals (including Hg) at the central coring site, particularly during lake recessions following erosion of
466 exposures around the crater rim (Blais and Kalff, 1995; Engstrom and Rose, 2013). However,
467 evidence for low Hg burial both prior to and during AI-1 in Lake Bosumtwi suggests that over multiple
468 millennia, changes in Hg supply to the BOS04-5B drill site were predominantly driven by atmospheric
469 inputs, with minimal contribution from catchment-sourced materials.

470

471 **5.2.2. ~73 to 0 ka**

472 The magnitude and frequency of variability in Hg_T and Hg_{AR} increases at ~73 (± 5) ka. This shift is
473 coeval with an increase in the lake's water level (**Fig. 4b**), and changing sedimentary TOC,
474 terrigenous material, and pollen concentrations all corroborate a broad increase in local moisture
475 availability, temperature, and humidity following deposition of the AI-1 unit (**Fig. 4**) (McKay, 2012;
476 Scholz et al., 2007; Shanahan et al., 2008b). Our data also shows a simultaneous increase in Hg_T ,
477 Hg_{AR} , and a decrease in detrital material concentrations following ~73 ka (**Fig. 4b, S5**), suggesting
478 that Hg supply temporarily exceeded the diluting effects of clastic materials following lake level rise.

479 Lake deepening generally increases water column stratification, limiting the effects of vertical
480 transport processes such as turbulent energy generated by surface winds and currents (Gulati et al.,
481 2017). Deeper, more anoxic conditions are therefore typically associated with more effective organic
482 carbon burial (Gulati et al., 2017; Schultze et al., 2017), coupled with more distinct formation of
483 distinct laminations (Zolitschka et al., 2015) and precipitation of authigenic carbonates such as
484 siderites (Swart, 2015). Given that elevated Hg_T and Hg_{AR} correlate most closely with TOC
485 enrichment in Lake Bosumtwi following ~73 ka (**Fig. 3a**), this could suggest that Hg drawdown was
486 moderated by an increase in organic matter availability and preservation, as an indirect function of
487 bottom water deoxygenation. Evidence for an inverse relationship between sedimentary Hg
488 concentration and hypolimnion oxygen content has been identified in a number of meromictic lake
489 systems across the world (e.g., Schultze et al., 2017; Tisserand et al., 2022), and provides further
490 support for our interpretation.

491 Geochemical evidence suggests sedimentary oxygen depletion became progressively greater in Lake
492 Bosumtwi following ~73 ka, culminating with sapropel formation between 12.4 and 3.7 ka. This unit
493 contains clear Hg_T enrichments relative to the rest of the core (**Fig. 2, 4a**), is extremely rich in organic
494 matter (~15-20%), and contains a high concentration of blue-green algae *Anabaena* deposits (Russell
495 et al., 2003). Sapropelic layers have emerged as key sites of Hg enrichment from a suite of marine
496 and lacustrine-based studies, which suggest this may be due to changes in productivity, sediment
497 oxygenation, and diagenetic processes (e.g., Frieling et al., 2023; Gehrke et al., 2009; Jeon et al.,
498 2020). Scavenging of Hg from the water column by algae is also a process now recognised as an
499 important driver of Hg export to lacustrine sediments; particularly in systems where primary
500 productivity, organic matter production, and burial capacity is high (Biestler et al., 2018; Schütze et al.,
501 2021). These conditions are met in Lake Bosumtwi following ~73 ka, meaning the observed changes



502 in sedimentary Hg_T could be linked to elevated rates of scavenging, as a function of enhanced
503 primary productivity.

504 In closed-basin lakes where fluxes of organic material from the catchment (e.g., soils and vegetation)
505 are minimal, measurable changes in sedimentary Hg concentration would require a simultaneous
506 increase in Hg fluxes to the system: to counterbalance Hg depletion by scavenging, methylation, or
507 evasion back to the atmosphere (e.g., Bravo et al., 2017; Hermanns et al., 2013; Outridge et al.,
508 2007; Schütze et al., 2021). For Lake Bosumtwi, these direct inputs may have come from
509 precipitation, and/or from increased flux of charcoal into the lake following local wildfire events (Cooke
510 et al., 2020).

511 Lake Bosumtwi records evidence for an increase in local precipitation following ~73 ka. Model and
512 proxy-based data show that the precipitation-evaporation balance is directly coupled to lake level in
513 this system, such that lake deepening occurs as a function of more rainfall (Shanahan et al., 2008b).
514 Proxy data generated from the BOS04-5B core suggest that progressively wetter conditions affected
515 the catchment following ~73 ka (e.g., Gosling et al., 2022a; Shanahan et al., 2008b), and were
516 produced by a broader, regional-scale shift in hydroclimate across sub-Saharan Africa (**Fig. 5**). These
517 records include deep drill cores from lakes Malawi (Tanzania), Bambili (Cameroon), Tanganyika
518 (Tanzania/Democratic Republic of the Congo), Chew Bahir (Ethiopia) and Chala (Tanzania) (e.g.,
519 Cohen et al., 2007; Foerster et al., 2022; Lézine et al., 2019; Scholz et al., 2007), and marine cores
520 extracted from the West African margin (**Figs. 1, 5**) (e.g., Kinsley et al., 2022; Skonieczny et al.,
521 2019). Therefore, a coeval increase in the frequency and amplitude of Hg enrichment in Lake
522 Bosumtwi, and associated rise in lake level, could indirectly reflect a regional-scale shift in
523 hydroclimate favouring wetter conditions in West Africa.

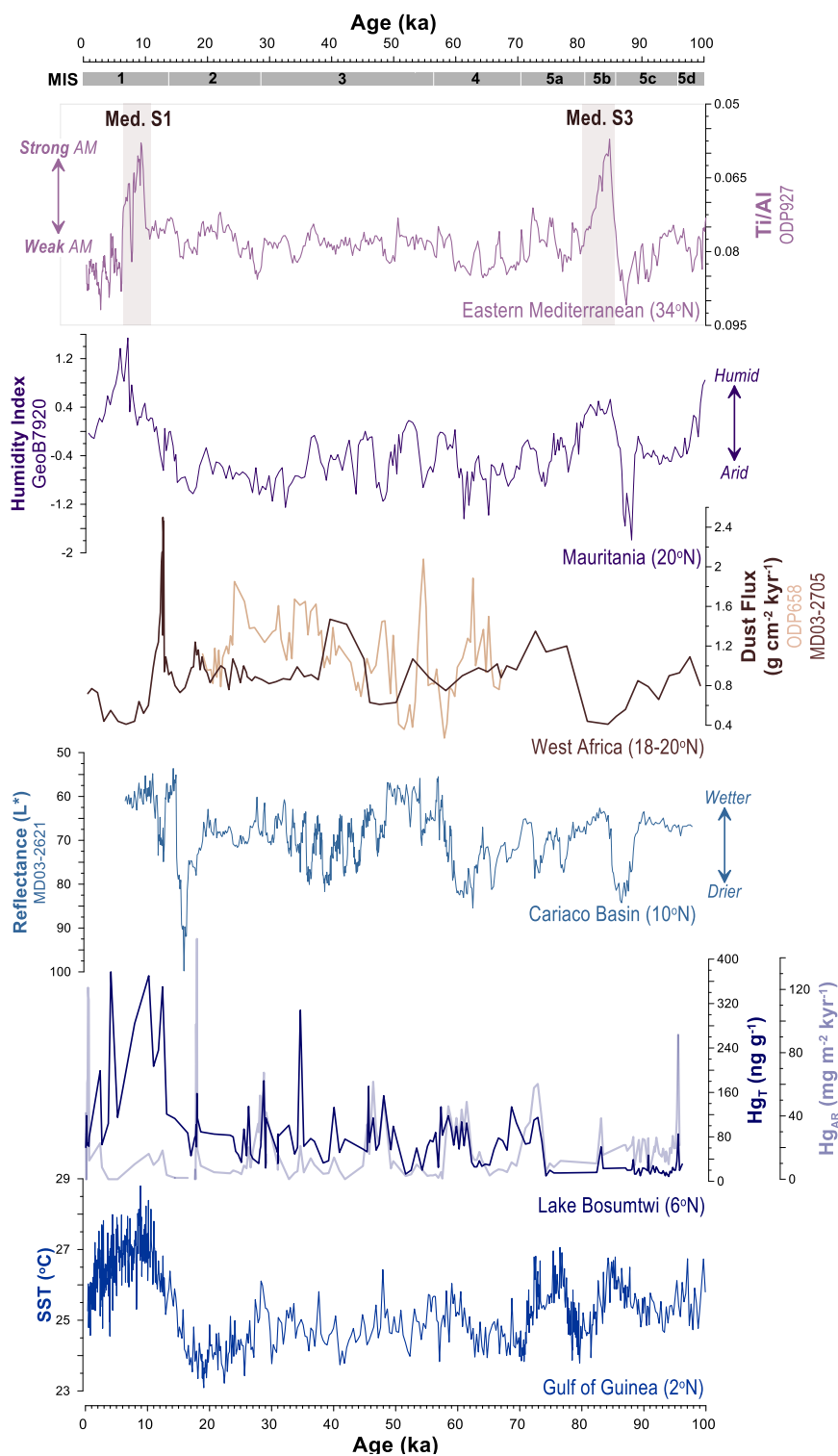




Figure 5: Records of total mercury (Hg_T) and mercury accumulation rate (Hg_{AR}) for Lake Bosumtwi generated by this study, compared with key paleoclimate records presented in order of latitude (physical locations shown in **Figure 1**). Sea-surface temperature (SST) reconstructed in core MD03-2707 from the Gulf of Guinea (Weldeab et al., 2007). Sediment total reflectance (L^*) in marine core MD03-2621 from offshore South America (Cariaco Basin, Venezuela) as a proxy for oscillations in mean ITCZ position, and hydrological conditions anticipated in light of these oscillations over West Africa (Deplazes et al., 2013). Dust fluxes recorded in cores ODP658 (Cap Blanc; Kinsley et al., 2022) and MD03-2705 (Skonieczny et al., 2019), and a continental humidity index of core GeoB7920-2 (Mauritanian seamount; Tjallingii et al., 2008) – all from offshore Mauritania. Finally, Ti/Al recorded in core ODP 927 from the Eastern Mediterranean as a record of riverine (low Ti/Al) versus aeolian (high Ti/Al) North African inputs to the Mediterranean basin, with low values reflecting a more intense African monsoon (Grant et al., 2022, 2017). Mediterranean sapropels one (Med. S1) and three (Med. S3) are marked by light brown bars (Grant et al., 2016). Light grey bars mark marine isotope stages (MIS) defined by the LR04 benthic marine isotope stack (Lisiecki and Raymo, 2005).

524

525 Hydroclimate was a dominant driver of changes in fire activity in sub-Saharan Africa during the late
526 Pleistocene. Wetter climatic conditions are typically associated with heightened fire activity due to
527 associated increases in terrestrial biomass (e.g., Gosling et al., 2021; Moore et al., 2022), and
528 wildfires are also a significant source of Hg, accounting for ~13% of natural Hg (re-)emissions to the
529 modern atmosphere (Francisco López et al., 2022). The influence of biomass burning on the Hg
530 record presented here is less clear; despite being a well-constrained factor in the Bosumtwi
531 catchment. No clear correlation is visible between Hg_T , Hg_{AR} , and two discrete macro- (Kiely, 2023)
532 and micro- (Miller et al., 2016) charcoal profiles generated from the BOS04-5B core, suggesting that
533 the effects of Hg emitted during wildfires did not leave a clear imprint on Hg variability in this record
534 (**Fig. S8**).

535

536 **6. Synthesis and conclusions**

537 This study seeks a better understanding of the impact that local, climate-driven environmental shifts
538 may have on the terrestrial Hg cycle over multiple millennia. The resolution of the BOS04-5B record
539 (~0.6 ka per sample) precludes a detailed assessment of more recent (<0.2-kyr), anthropogenic-
540 driven changes in local Hg cycling. However, this record is well suited for a broader exploration of
541 patterns and drivers of variability in sedimentary Hg concentrations in Lake Bosumtwi during the late
542 Pleistocene. Combining our results with existing data reveals two possible drivers of variability in Hg_T
543 and Hg_{AR} in Lake Bosumtwi on these timescales: organic matter (host) availability, and local-scale
544 changes in Hg input to the lake by precipitation (**Fig. 4**). Both are intrinsically coupled to the local
545 hydroclimate by their link to the lake level, with higher lake levels typically corresponding to wetter
546 conditions in the catchment, and deposition of more organic-rich sediments. **Figure 6** illustrates how
547 selected environmental processes, under different environmental conditions, may have interacted with
548 these two drivers to control Hg burial in Lake Bosumtwi between ~96 and 0 ka. Considered together,
549 the evidence summarised in panels **(1)**, **(2)**, and **(2a)** all suggest that rates of Hg drawdown in Lake



550 Bosumtwi, and indeed the signals retained in the sediment record, reflect changes in net Hg supply
551 from the atmosphere.

552 Between ~96 and 73 ka (**Fig. 6, panel (1)**), generally arid conditions shifted the lake into a negative
553 water balance. Not only could this have reduced the net flux of Hg to the lake by wet deposition
554 (precipitation), but a negative water balance would also limit internal primary productivity and
555 preservation, and so render less organic material available to sequester any Hg present in the
556 system. Secondary dilution of Hg by detrital materials could have also lowered sedimentary Hg
557 concentrations, with elevated sediment delivery to the BOS04 site driven by exposure of the steep-
558 sided crater walls during lake level lowering, and heightened soil instability due to widespread
559 recession of catchment vegetation. All would persist (if not strengthen) during AI-1, and so could
560 explain the lack of any measurable changes in Hg_T and Hg_{AR} during this time.

561 Following an extended period of aridity, net supply of Hg to the basin would be increased by
562 precipitation following ~73 ka, which would simultaneously cause the lake to become deeper and
563 more stratified (**Fig. 6, panel (2)**). As the bottom waters became more oxygen-depleted, more
564 effective organic matter burial would simultaneously enhance Hg drawdown compared to detrital
565 mineral supply; with higher lake levels, vegetation growth, and soil stabilization preventing exposure
566 and erosion of the crater walls and soils surrounding the lake. Hence, this abrupt shift to humid (net-
567 positive precipitation-evaporation balance) conditions in the Bosumtwi catchment could plausibly have
568 driven an increase in sedimentary Hg concentrations and accumulation, by eliciting a pronounced rise
569 in lake level as well as increasing the atmospheric Hg flux.

570 The processes described in panel (2) would be amplified further between ~15 and 4 ka (**Fig. 6, panel**
571 **2a**). Corresponding to Bosumtwi sapropel unit 1, this unit marks a distinct humid period characterised
572 by anomalously high rainfall, and documented by proxy records across sub-Saharan Africa
573 (Shanahan et al., 2015). For a closed lake system such as Lake Bosumtwi, these wetter conditions
574 would drive a sharp increase in lake depth, stratification, and scavenging in the water column – all of
575 which could favour heightened Hg drawdown to the sediment. ‘Flattening’ of the Hg-TOC relationship
576 during this interval also suggests that the Hg supply was (far) exceeded by the organic matter
577 availability (**Fig. S3a**), and so elevated Hg supply by precipitation could explain why Hg_T and Hg_{AR}
578 values are so unusually high (**Fig. 4a, 5**).

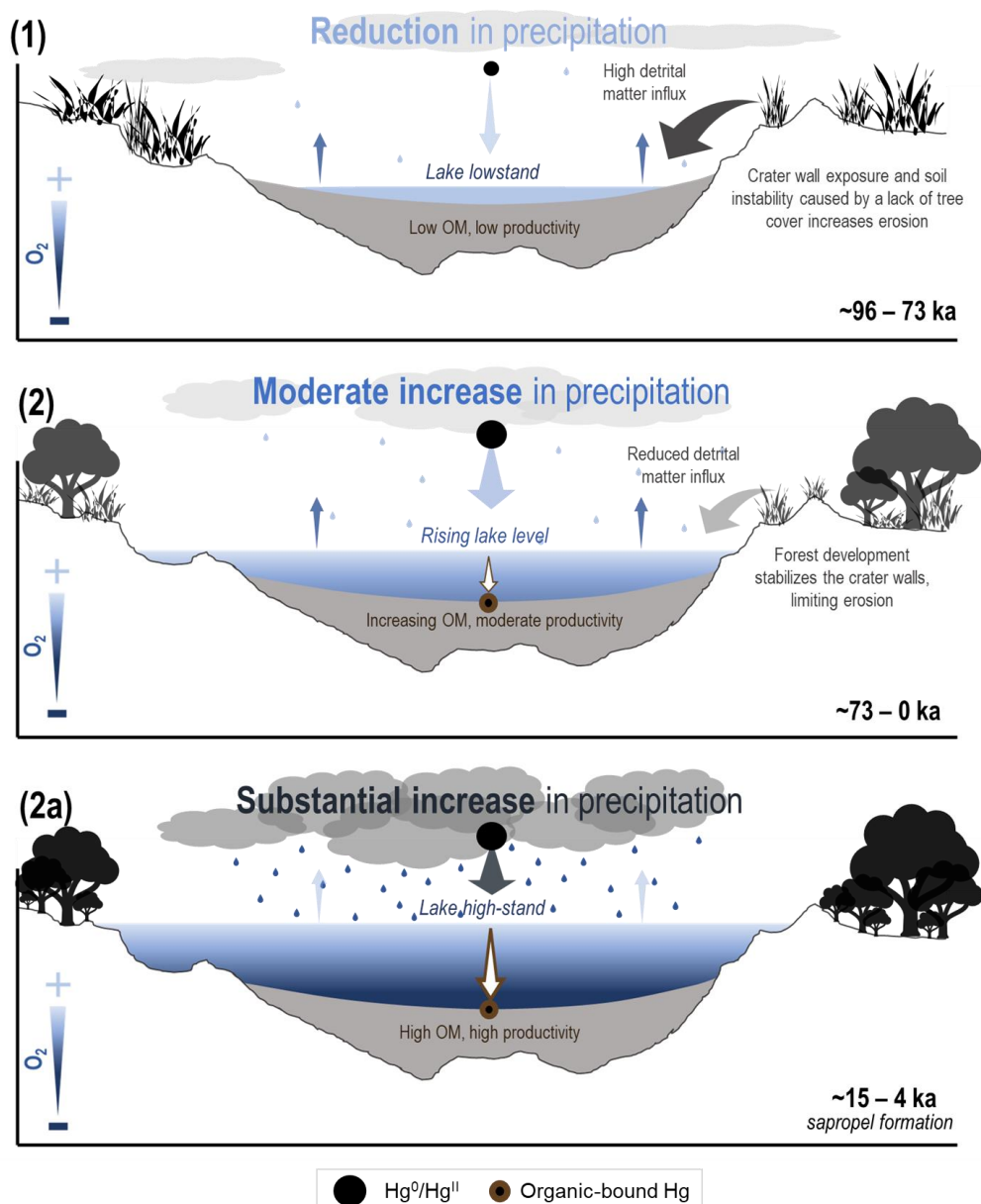


Figure 6: Schematic model depicting the processes that may control Hg flux, accumulation, and burial in Lake Bosumtwi under (1) arid (~93 – 73 ka), and (2) humid (~73 – 0 ka), environmental conditions. Panel (2a) depicts the very humid conditions that would be conducive to sapropel formation, such as those known to have occurred during the African Humid Period (~15 – 4 ka). Taken together, Hg fluxes increase during wet periods due to higher wet deposition directly to the lake relative to evasion, and/or by enhanced mobilization and transport of Hg from the catchment. Hg sequestration can also be enhanced by OM-scavenging in the water column, and increased lake stratification (anoxia at lake floor). The opposite occurs during dry intervals.



579 Future research should seek better constraints on how basin-specific variations in sediment
580 composition, lake structure, and water balance may influence how sedimentary Hg signals are
581 preserved and interpreted. This is because all could produce diverse, and perhaps contrasting, results
582 between lake systems. For example, results from Lake Bosumtwi suggest that lakes with smaller
583 watersheds, simple morphology, and minimal hydrological connectivity to the catchment could be
584 suitable targets to study catchment and intra-lake depositional processes over multiple millennia.
585 However, there are currently too few records covering these timescales to say this with certainty, and
586 not all closed lakes record measurable changes in Hg composition corresponding to changes in local
587 hydroclimate (Lent and Alexander, 1996; Pompeani et al., 2018). Organic matter/host phase
588 availability also appears to represent just one of several possible processes governing Hg burial in
589 lacustrine systems, given these systems are more readily affected by short-term changes in erosion,
590 nutrients, water balance, and catchment hydrology (Paine et al., 2024; Schütze et al., 2021).

591 Lake Bosumtwi is a small, morphologically simple lake. However, the complexity shown by its
592 sedimentary Hg record suggests that identical stratigraphic signals are unlikely to be recorded in
593 separate lakes, even if they are dominated by one common process, mechanism, and/or structure.
594 Exploring the importance of hydroclimate for Hg cycling relative to different catchment to lake area
595 ratios, hydrology (e.g., endorheic (closed) versus exoreic (open)), and/or catchment structures (e.g.,
596 forest versus savannah) would undoubtedly help to better resolve processes acting on single
597 lacustrine and terrestrial successions, but also identify the systems that may more sensitively record
598 major changes in Hg cycling.

599 This study provides new and valuable evidence for long-term interactions between terrestrial Hg
600 cycling and hydroclimate, and demonstrates that hydroclimate may be a key driver of Hg cycling in
601 tropical lakes over millennial-timescales. The sparse number of continuous, pre-industrial Hg records
602 currently available for sub-Saharan Africa have historically limited the ability to understand the extent
603 to which hydroclimate may drive long-term ($>10^2$ -year) variability in the Hg cycle (Schneider et al.,
604 2023), and subsequently how this relationship is represented in local and global ecosystem models
605 (Cooke et al., 2020; Obrist et al., 2018). Although this knowledge gap cannot be satisfied by a single
606 record, study of Lake Bosumtwi reinforces the value of these records for better characterization of the
607 Hg behaviour likely to be associated with projected future, monsoon-driven, hydroclimate variability
608 (Chang et al., 2022). In time, this could translate to better understanding of how the tropical Hg cycle
609 may respond to future, global-scale changes (Gustin et al., 2020; Schneider et al., 2023).

610

611 **Competing Interests**

612 The contact author has declared that none of the authors has any competing interests.

613 **Acknowledgements**

614 ARP, IMF, JF, and TAM acknowledge funding from European Research Council Consolidator Grant
615 V-ECHO (ERC-2018-COG-8187 17-V-ECHO). ARP thanks Christopher Scholz for provision of



616 sediment data, alongside James Bryson, Alex Dickson, and Erdem Idiz for insightful discussions in
617 early stages of manuscript preparation. Thanks also go to Stephen Wyatt (University of Oxford) for
618 analytical assistance throughout the study. All authors thank members of the International Continental
619 Scientific Drilling Program Lake Bosumtwi Drilling Project: for their efforts in extracting and producing
620 the sediment succession, and making the data available for scientific use.

621

622 References

- 623 Åkerblom, S., Bishop, K., Björn, E., Lambertsson, L., Eriksson, T., Nilsson, M.B., 2013. Significant interaction
624 effects from sulfate deposition and climate on sulfur concentrations constitute major controls on
625 methylmercury production in peatlands. *Geochimica et Cosmochimica Acta* 102, 1–11.
626 <https://doi.org/10.1016/j.gca.2012.10.025>
- 627 Amos, H.M., Sonke, J.E., Obrist, D., Robins, N., Hagan, N., Horowitz, H.M., Mason, R.P., Witt, M., Hedgecock,
628 I.M., Corbitt, E.S., Sunderland, E.M., 2015. Observational and modeling constraints on global
629 anthropogenic enrichment of mercury. *Environmental Science and Technology* 49, 4036–4047.
630 <https://doi.org/10.1021/es5058665>
- 631 Armenteros, I., 2010. Diagenesis of Carbonates in Continental Settings, in: *Developments in Sedimentology*.
632 Elsevier, pp. 61–151. [https://doi.org/10.1016/S0070-4571\(09\)06202-5](https://doi.org/10.1016/S0070-4571(09)06202-5)
- 633 Armstrong, E., Tallavaara, M., Hopcroft, P.O., Valdes, P.J., 2023. North African humid periods over the past
634 800,000 years. *Nat Commun* 14, 5549. <https://doi.org/10.1038/s41467-023-41219-4>
- 635 Benoit, J.M., Gilmour, C.C., Mason, R.P., Heyes, A., 1999. Sulfide controls on mercury speciation and
636 bioavailability to methylating bacteria in sediment pore water. *Environmental Science and Technology*
637 33, 1780. <https://doi.org/10.1021/es992007q>
- 638 Biester, H., Pérez-Rodríguez, M., Gilfedder, B.-S., Martínez Cortizas, A., Hermanns, Y.-M., 2018. Solar
639 irradiance and primary productivity controlled mercury accumulation in sediments of a remote lake in the
640 Southern Hemisphere during the past 4000 years: Primary productivity and mercury accumulation.
641 *Limnol. Oceanogr.* 63, 540–549. <https://doi.org/10.1002/lno.10647>
- 642 Bin, C., Xiaoru, W., Lee, F.S.C., 2001. Pyrolysis coupled with atomic absorption spectrometry for the
643 determination of mercury in Chinese medicinal materials. *Analytica Chimica Acta* 447, 161–169.
644 [https://doi.org/10.1016/S0003-2670\(01\)01218-1](https://doi.org/10.1016/S0003-2670(01)01218-1)
- 645 Bishop, K., Shanley, J.B., Riscassi, A., de Wit, H.A., Eklöf, K., Meng, B., Mitchell, C., Osterwalder, S., Schuster,
646 P.F., Webster, J., Zhu, W., 2020. Recent advances in understanding and measurement of mercury in
647 the environment: Terrestrial Hg cycling. *Science of the Total Environment* 721.
648 <https://doi.org/10.1016/j.scitotenv.2020.137647>
- 649 Blais, J.M., Kalff, J., 1995. The influence of lake morphometry on sediment focusing. *Limnol. Oceanogr.* 40, 582–
650 588. <https://doi.org/10.4319/lo.1995.40.3.0582>
- 651 Boamah, D., Koeberl, C., 2007. The Lake Bosumtwi impact structure in Ghana: A brief environmental
652 assessment and discussion of ecotourism potential. *Meteoritics and Planetary Science* 42, 561–567.
653 <https://doi.org/10.1111/j.1945-5100.2007.tb01061.x>
- 654 Bradley, R.S., Diaz, H.F., 2021. Late Quaternary Abrupt Climate Change in the Tropics and Sub-Tropics: The
655 Continental Signal of Tropical Hydroclimatic Events (THEs). *Reviews of Geophysics* 59,
656 e2020RG000732. <https://doi.org/10.1029/2020RG000732>
- 657 Branfireun, B.A., Cosio, C., Poulain, A.J., Riise, G., Bravo, A.G., 2020. Mercury cycling in freshwater systems -
658 An updated conceptual model. *Science of the Total Environment* 745.
659 <https://doi.org/10.1016/j.scitotenv.2020.140906>
- 660 Bravo, A.G., Bouchet, S., Tolu, J., Björn, E., Mateos-Rivera, A., Bertilsson, S., 2017. Molecular composition of
661 organic matter controls methylmercury formation in boreal lakes. *Nat Commun* 8, 14255.
662 <https://doi.org/10.1038/ncomms14255>
- 663 Brodie, C.R., Leng, M.J., Casford, J.S.L., Kendrick, C.P., Lloyd, J.M., Yongqiang, Z., Bird, M.I., 2011. Evidence
664 for bias in C and N concentrations and $\delta^{13}\text{C}$ composition of terrestrial and aquatic organic materials due
665 to pre-analysis acid preparation methods. *Chemical Geology* 282, 67–83.
666 <https://doi.org/10.1016/j.chemgeo.2011.01.007>
- 667 Brooks, K., Scholz, C.A., King, J.W., Peck, J., Overpeck, J.T., Russell, J.M., Amoako, P.Y.O., 2005. Late-
668 Quaternary lowstands of lake Bosumtwi, Ghana: Evidence from high-resolution seismic-reflection and
669 sediment-core data. *Palaeogeography, Palaeoclimatology, Palaeoecology* 216, 235–249.
670 <https://doi.org/10.1016/j.palaeo.2004.10.005>
- 671 Brumsack, H.J., 2006. The trace metal content of recent organic carbon-rich sediments: Implications for
672 Cretaceous black shale formation. *Palaeogeography, Palaeoclimatology, Palaeoecology* 232, 344–361.
673 <https://doi.org/10.1016/j.palaeo.2005.05.011>
- 674 Chang, M., Liu, B., Wang, B., Martinez-Villalobos, C., Ren, G., Zhou, T., 2022. Understanding Future Increases
675 in Precipitation Extremes in Global Land Monsoon Regions. *Journal of Climate* 35, 1839–1851.
676 <https://doi.org/10.1175/JCLI-D-21-0409.1>



- 677 Chede, B.S., Venancio, I.M., Figueiredo, T.S., Albuquerque, A.L.S., Silva-Filho, E.V., 2022. Mercury deposition in
678 the western tropical South Atlantic during the last 70 ka. *Palaeogeography, Palaeoclimatology,*
679 *Palaeoecology* 601, 111122. <https://doi.org/10.1016/j.palaeo.2022.111122>
- 680 Cohen, A., Campisano, C., Arrowsmith, R., Asrat, A., Behrensmeyer, A.K., Deino, A., Feibel, C., Hill, A.,
681 Johnson, R., Kingston, J., Lamb, H., Lowenstein, T., Noren, A., Olago, D., Owen, R.B., Potts, R., Reed,
682 K., Renaut, R., Schäbitz, F., Tiercelin, J.-J., Trauth, M.H., Wynn, J., Ivory, S., Brady, K., O'Grady, R.,
683 Rodysill, J., Githiri, J., Russell, J., Foerster, V., Dommain, R., Rucina, S., Deocampo, D., Russell, J.,
684 Billingsley, A., Beck, C., Dorenbeck, G., Dullo, L., Feary, D., Garello, D., Gromig, R., Johnson, T.,
685 Junginger, A., Karanja, M., Kimburi, E., Mbuthia, A., McCartney, T., McNulty, E., Muiruri, V., Nambiro,
686 E., Negash, E.W., Njagi, D., Wilson, J.N., Rabideaux, N., Raub, T., Sier, M.J., Smith, P., Urban, J.,
687 Warren, M., Yadeta, M., Yost, C., Zinaye, B., 2016. The Hominin Sites and Paleolakes Drilling Project:
688 inferring the environmental context of human evolution from eastern African rift lake deposits. *Scientific*
689 *Drilling* 21, 1–16. <https://doi.org/10.5194/sd-21-1-2016>
- 690 Cohen, A.S., Campisano, C.J., Arrowsmith, J.R., Asrat, A., Beck, C.C., Behrensmeyer, A.K., Deino, A.L., Feibel,
691 C.S., Foerster, V., Kingston, J.D., Lamb, H.F., Lowenstein, T.K., Lupien, R.L., Muiruri, V., Olago, D.O.,
692 Owen, R.B., Potts, R., Russell, J.M., Schaebitz, F., Stone, J.R., Trauth, M.H., Yost, C.L., 2022.
693 Reconstructing the Environmental Context of Human Origins in Eastern Africa Through Scientific
694 Drilling. *Annu. Rev. Earth Planet. Sci.* 50, 451–476. [https://doi.org/10.1146/annurev-earth-031920-](https://doi.org/10.1146/annurev-earth-031920-081947)
695 [081947](https://doi.org/10.1146/annurev-earth-031920-081947)
- 696 Cohen, A.S., Stone, J.R., Beuning, K.R.M., Park, L.E., Reinthal, P.N., Dettman, D., Scholz, C.A., Johnson, T.C.,
697 King, J.W., Talbot, M.R., Brown, E.T., Ivory, S.J., 2007. Ecological consequences of early Late
698 Pleistocene megadroughts in tropical Africa. *PNAS U.S.A.* 104, 16422–16427.
699 <https://doi.org/10.1073/pnas.0703873104>
- 700 Cooke, C.A., Martínez-Cortizas, A., Bindler, R., Sexauer Gustin, M., 2020. Environmental archives of
701 atmospheric Hg deposition – A review. *Science of the Total Environment* 709, 134800.
702 <https://doi.org/10.1016/j.scitotenv.2019.134800>
- 703 Deplazes, G., Lückge, A., Peterson, L.C., Timmermann, A., Hamann, Y., Hughen, K.A., Röhl, U., Laj, C., Cane,
704 M.A., Sigman, D.M., Haug, G.H., 2013. Links between tropical rainfall and North Atlantic climate during
705 the last glacial period. *Nature Geoscience* 6, 213–217. <https://doi.org/10.1038/ngeo1712>
- 706 Edwards, B.A., Kushner, D.S., Outridge, P.M., Wang, F., 2021. Fifty years of volcanic mercury emission
707 research: Knowledge gaps and future directions. *Science of the Total Environment* 757, 143800.
708 <https://doi.org/10.1016/j.scitotenv.2020.143800>
- 709 Engstrom, D.R., Rose, N.L., 2013. A whole-basin, mass-balance approach to paleolimnology. *J Paleolimnol* 49,
710 333–347. <https://doi.org/10.1007/s10933-012-9675-5>
- 711 Fadina, O.A., Venancio, I.M., Belem, A., Silveira, C.S., Bertagnolli, D. de C., Silva-Filho, E.V., Albuquerque,
712 A.L.S., 2019. Paleoclimatic controls on mercury deposition in northeast Brazil since the Last Interglacial.
713 *Quaternary Science Reviews* 221, 105869. <https://doi.org/10.1016/j.quascirev.2019.105869>
- 714 Figueiredo, T.S., Bergquist, B.A., Santos, T.P., Albuquerque, A.L.S., Silva-Filho, E.V., 2022. Relationship
715 between glacial CO2 drawdown and mercury cycling in the western South Atlantic: An isotopic insight.
716 *Geology* 50, 3–7. <https://doi.org/10.1130/g49942.1>
- 717 Foerster, V., Asrat, A., Bronk Ramsey, C., Brown, E.T., Chapot, M.S., Deino, A., Duesing, W., Grove, M., Hahn,
718 A., Junginger, A., Kaboth-Bahr, S., Lane, C.S., Opitz, S., Noren, A., Roberts, H.M., Stockhecke, M.,
719 Tiedemann, R., Vidal, C.M., Vogelsang, R., Cohen, A.S., Lamb, H.F., Schaebitz, F., Trauth, M.H., 2022.
720 Pleistocene climate variability in eastern Africa influenced hominin evolution. *Nature Geoscience* 15,
721 805–811. <https://doi.org/10.1038/s41561-022-01032-y>
- 722 Francisco López, A., Heckenauer Barrón, E.G., Bello Bugallo, P.M., 2022. Contribution to understanding the
723 influence of fires on the mercury cycle: Systematic review, dynamic modelling and application to
724 sustainable hypothetical scenarios. *Environmental Monitoring & Assessment* 194, 707.
725 <https://doi.org/10.1007/s10661-022-10208-3>
- 726 Frieling, J., Mather, T.A., März, C., Jenkyns, H.C., Hennekam, R., Reichart, G.-J., Slomp, C.P., Van Helmond,
727 N.A.G.M., 2023. Effects of redox variability and early diagenesis on marine sedimentary Hg records.
728 *Geochimica et Cosmochimica Acta* S0016703723001850. <https://doi.org/10.1016/j.gca.2023.04.015>
- 729 Gehrke, G.E., Blum, J.D., Meyers, P.A., 2009. The geochemical behavior and isotopic composition of Hg in a
730 mid-Pleistocene western Mediterranean sapropel. *Geochimica et Cosmochimica Acta* 73, 1651–1665.
731 <https://doi.org/10.1016/j.gca.2008.12.012>
- 732 Gosling, W.D., McMichael, C.N.H., Groenwoud, Z., Roding, E., Miller, C.S., Julier, A.C.M., 2021. Preliminary
733 evidence for green, brown and black worlds in tropical western Africa during the Middle and Late
734 Pleistocene. *Palaeoecology of Africa* 35, 13–25. <https://doi.org/10.1201/9781003162766>
- 735 Gosling, W.D., Miller, C.S., Shanahan, T.M., Holden, P.B., Overpeck, J.T., van Langevelde, Frank., 2022a. A
736 stronger role for long-term moisture change than for CO2 in determining tropical woody vegetation
737 change. *Science* 376, 653–656. <https://doi.org/10.1126/science.abg4618>
- 738 Gosling, W.D., Scerri, E.M.L., Kaboth-Bahr, S., 2022b. The climate and vegetation backdrop to hominin evolution
739 in Africa. *Philosophical Transactions of the Royal Society B: Biological Sciences* 377.
740 <https://doi.org/10.1098/rstb.2020.0483>
- 741 Grant, K.M., Amarathunga, U., Amies, J.D., Hu, P., Qian, Y., Penny, T., Rodriguez-Sanz, L., Zhao, X., Heslop,
742 D., Liebrand, D., Hennekam, R., Westerhold, T., Gilmore, S., Lourens, L.J., Roberts, A.P., Rohling, E.J.,



- 743 2022. Organic carbon burial in Mediterranean sapropels intensified during Green Sahara Periods since
744 3.2 Myr ago. *Communications Earth & Environment* 3, 11. <https://doi.org/10.1038/s43247-021-00339-9>
- 745 Grant, K.M., Grimm, R., Mikolajewicz, U., Marino, G., Ziegler, M., Rohling, E.J., 2016. The timing of
746 Mediterranean sapropel deposition relative to insolation, sea-level and African monsoon changes.
747 *Quaternary Science Reviews* 140, 125–141. <https://doi.org/10.1016/j.quascirev.2016.03.026>
- 748 Grant, K.M., Rohling, E.J., Westerhold, T., Zabel, M., Heslop, D., Konijnendijk, T., Lourens, L., 2017. A 3 million
749 year index for North African humidity/aridity and the implication of potential pan-African Humid periods.
750 *Quaternary Science Reviews* 171, 100–118. <https://doi.org/10.1016/j.quascirev.2017.07.005>
- 751 Grygar, T.M., Mach, K., Martinez, M., 2019. Checklist for the use of potassium concentrations in siliciclastic
752 sediments as paleoenvironmental archives. *Sedimentary Geology* 382, 75–84.
753 <https://doi.org/10.1016/j.sedgeo.2019.01.010>
- 754 Guédron, S., Ledru, M.P., Escobar-Torrez, K., Develle, A.L., Brisset, E., 2018. Enhanced mercury deposition by
755 Amazonian orographic precipitation: Evidence from high-elevation Holocene records of the Lake
756 Titicaca region (Bolivia). *Palaeogeography, Palaeoclimatology, Palaeoecology* 511, 577–587.
757 <https://doi.org/10.1016/j.palaeo.2018.09.023>
- 758 Gulati, R.D., Zadereev, E.S., Degermendzhi, A.G. (Eds.), 2017. *Ecology of Meromictic Lakes*, Ecological Studies.
759 Springer International Publishing, Cham. <https://doi.org/10.1007/978-3-319-49143-1>
- 760 Gustin, M.S., Bank, M.S., Bishop, K., Bowman, K., Branfireun, B., Chételat, J., Eckley, C.S., Hammerschmidt,
761 C.R., Lamborg, C., Lyman, S., Martínez-Cortizas, A., Sommar, J., Tsui, M.T.-K., Zhang, T., 2020.
762 Mercury biogeochemical cycling: A synthesis of recent scientific advances. *Science of The Total*
763 *Environment* 737, 139619. <https://doi.org/10.1016/j.scitotenv.2020.139619>
- 764 Han, S., Obratzsova, A., Pretto, P., Deheyn, D.D., Gieskes, J., Tebo, B.M., 2008. Sulfide and iron control on
765 mercury speciation in anoxic estuarine sediment slurries. *Marine Chemistry* 111, 214–220.
766 <https://doi.org/10.1016/j.marchem.2008.05.002>
- 767 Hermanns, Y.M., Biester, H., 2013. A 17,300-year record of mercury accumulation in a pristine lake in southern
768 Chile. *Journal of Paleolimnology* 49, 547–561. <https://doi.org/10.1007/s10933-012-9668-4>
- 769 Hermanns, Y.M., Cortizas, A.M., Arz, H., Stein, R., Biester, H., 2013. Untangling the influence of in-lake
770 productivity and terrestrial organic matter flux on 4,250 years of mercury accumulation in Lake Hambre,
771 Southern Chile. *Journal of Paleolimnology* 49, 563–573. <https://doi.org/10.1007/s10933-012-9657-7>
- 772 Hernández, A., Martín-Puertas, C., Moffa-Sánchez, P., Moreno-Chamarro, E., Ortega, P., Blockley, S., Cobb, K.,
773 Comas-Bru, L., Giralt, S., Goosse, H., Luterbacher, J., Martrat, B., Muscheler, R., Parnell, A., Pla-
774 Rabes, S., Sjolte, J., Scaife, A., Swingedouw, D., Wise, E., Xu, G., 2020. Modes of climate variability:
775 Synthesis and review of proxy-based reconstructions through the Holocene. *Earth-Science Reviews*
776 209, 103286. <https://doi.org/10.1016/j.earscirev.2020.103286>
- 777 Hsu-Kim, H., Kucharzyk, K.H., Zhang, T., Deshusses, M.A., 2013. Mechanisms Regulating Mercury
778 Bioavailability for Methylating Microorganisms in the Aquatic Environment: A Critical Review.
779 *Environmental Science & Technology* 47, 2441–2456. <https://doi.org/10.1021/es304370g>
- 780 Jenkyns, H.C., 1988. The Early Toarcian (Jurassic) Anoxic Event. *American Journal of Science*.
- 781 Jenkyns, H.C., Weedon, G.P., 2013. Chemostratigraphy (CaCO₃, TOC, δ¹³C_{org}) of Sinemurian (Lower Jurassic)
782 black shales from the Wessex Basin, Dorset and palaeoenvironmental implications. *Newsletters on*
783 *Stratigraphy* 46, 1–21. <https://doi.org/10.1127/0078-0421/2013/0029>
- 784 Jeon, B., Scirde, A., Cizdziel, J.V., Chen, J., Black, O., Wallace, D.J., Zhou, Y., Lepak, R.F., Hurley, J.P., 2020.
785 Historical deposition of trace metals in a marine sapropel from Mangrove Lake, Bermuda with emphasis
786 on mercury, lead, and their isotopic composition. *Journal of Soils & Sediments* 20, 2266–2276.
787 <https://doi.org/10.1007/s11368-020-02567-6>
- 788 Jourdan, F., Renne, P.R., Reimold, W.U., 2009. An appraisal of the ages of terrestrial impact structures. *Earth*
789 *and Planetary Science Letters* 286, 1–13. <https://doi.org/10.1016/j.epsl.2009.07.009>
- 790 Kaboth-Bahr, S., Gosling, W.D., Vogelsang, R., Bahr, A., Scerri, E.M.L., 2021. Paleo-ENSO influence on African
791 environments and early modern humans. *PNAS* 118, 1–6. <https://doi.org/10.1073/pnas.2018277118>
- 792 Kiely, R., 2023. A 50,000-year reconstruction of West African fire history (MSc Thesis). University of Amsterdam,
793 Amsterdam.
- 794 Kinsley, C.W., Bradtmiller, L.I., McGee, D., Galgay, M., Stuut, J.B., Tjallingii, R., Winckler, G., DeMenocal, P.B.,
795 2022. Orbital and Millennial-Scale Variability in Northwest African Dust Emissions Over the Past 67,000
796 years. *Paleoceanography and Paleoclimatology* 37, 1–22. <https://doi.org/10.1029/2020PA004137>
- 797 Koeberl, C., Milkereit, B., Overpeck, J.T., Scholz, C.A., Amoako, P.Y.O., Boamah, D., Danuor, S.K., Karp, T.,
798 Kueck, J., Hecky, R.E., King, J.W., Peack, J.A., 2007. An international and multidisciplinary drilling
799 project into a young complex impact structure: The 2004 ICDP Bosumtwi Crater Drilling Project - An
800 overview. *Meteoritics and Planetary Science* 42, 483–511. <https://doi.org/10.1111/j.1945-5100.2007.tb01057.x>
- 801 Koeberl, C., Peck, J., King, J., Milkereit, B., Overpeck, J., Scholz, C., 2005. The ICDP lake Bosumtwi drilling
802 project: A first report. *Scientific Drilling* 1, 23–27. <https://doi.org/10.2204/iodp.sd.1.04.2005>
- 803 Kuss, J., Zülicke, C., Pohl, C., Schneider, B., 2011. Atlantic mercury emission determined from continuous
804 analysis of the elemental mercury sea-air concentration difference within transects between 50°N and
805 50°S. *Global Biogeochemical Cycles* 25. <https://doi.org/10.1029/2010GB003998>
- 806 Larrasoña, J.C., Roberts, A.P., Rohling, E.J., 2013. Dynamics of Green Sahara Periods and Their Role in
807 Hominin Evolution. *PLoS ONE* 8. <https://doi.org/10.1371/journal.pone.0076514>
- 808



- 809 Laskar, J., Robutel, P., Joutel, F., Gastineau, M., Correia, A.C.M., Levrard, B., 2004. A long-term numerical
810 solution for the insolation quantities of the Earth. *Astronomy and Astrophysics* 428, 261–285.
811 <https://doi.org/10.1051/0004-6361:20041335>
- 812 Leiva González, J., Diaz-Robles, L.A., Cereceda-Balic, F., Pino-Cortés, E., Campos, V., 2022. Atmospheric
813 Modelling of Mercury in the Southern Hemisphere and Future Research Needs: A Review. *Atmosphere*
814 13, 1226. <https://doi.org/10.3390/atmos13081226>
- 815 Lent, R.M., Alexander, C.R., 1996. Mercury accumulation in Devils Lake, north Dakota - effects of environmental
816 variation in closed-basin lakes on mercury chronologies. *Water, Air, & Soil Pollution* 98, 275–296.
- 817 Lézine, A.-M., Izumi, K., Kageyama, M., Achoundong, G., 2019. A 90,000-year record of Afromontane forest
818 responses to climate change. *Science* 363, 177–181. <https://doi.org/10.1126/science.aav6821>
- 819 Li, F., Ma, C., Zhang, P., 2020. Mercury Deposition, Climate Change and Anthropogenic Activities: A Review.
820 *Frontiers in Earth Science* 8, 316. <https://doi.org/10.3389/feart.2020.00316>
- 821 Lisiecki, L.E., Raymo, M.E., 2005. A Pliocene-Pleistocene stack of 57 globally distributed benthic $\delta^{18}O$ records.
822 *Paleoceanography* 20, 1–17. <https://doi.org/10.1029/2004PA001071>
- 823 Liu, M., Zhang, Q., Maavara, T., Liu, S., Wang, X., Raymond, P.A., 2021. Rivers as the largest source of mercury
824 to coastal oceans worldwide. *Nature Geoscience* 14, 672–677. <https://doi.org/10.1038/s41561-021-00793-2>
- 825
- 826 Lyman, S.N., Cheng, I., Gratz, L.E., Weiss-Penzias, P., Zhang, L., 2020. An updated review of atmospheric
827 mercury. *Science of the Total Environment* 707, 135575. <https://doi.org/10.1016/j.scitotenv.2019.135575>
- 828 Machado, W., Sanders, C.J., Santos, I.R., Sanders, L.M., Silva-Filho, E.V., Luiz-Silva, W., 2016. Mercury dilution
829 by autochthonous organic matter in a fertilized mangrove wetland. *Environmental Pollution* 213, 30–35.
830 <https://doi.org/10.1016/j.envpol.2016.02.002>
- 831 Mason, R.P., Laporte, J.M., Andres, S., 2000. Factors controlling the bioaccumulation of mercury,
832 methylmercury, arsenic, selenium, and cadmium by freshwater invertebrates and fish. *Archives of*
833 *Environmental Contamination and Toxicology* 38, 283–297. <https://doi.org/10.1007/s002449910038>
- 834 McKay, N.P., 2012. A multidisciplinary approach to late Quaternary paleoclimatology with an emphasis on sub-
835 saharan West Africa and the last interglacial period (PhD Thesis). University of Arizona, Arizona.
- 836 Menviel, L., Govin, A., Avenas, A., Meissner, K.J., Grant, K.M., Tzedakis, P.C., 2021. Drivers of the evolution and
837 amplitude of African Humid Periods. *Communications Earth & Environment* 2, 237.
838 <https://doi.org/10.1038/s43247-021-00309-1>
- 839 Miller, C.S., Gosling, W.D., 2014. Quaternary forest associations in lowland tropical West Africa. *Quaternary*
840 *Science Reviews* 84, 7–25. <https://doi.org/10.1016/j.quascirev.2013.10.027>
- 841 Miller, C.S., Gosling, W.D., Kemp, D.B., Coe, A.L., Gilmour, I., 2016. Drivers of ecosystem and climate change in
842 tropical West Africa over the past ~540 000 years. *Journal of Quaternary Science* 31, 671–677.
843 <https://doi.org/10.1002/jqs.2893>
- 844 Moore, H.R., Crocker, A.J., Belcher, C.M., Meckler, A.N., Osborne, C.P., Beerling, D.J., Wilson, P.A., 2022.
845 Hydroclimate variability was the main control on fire activity in northern Africa over the last 50,000 years.
846 *Quaternary Science Reviews* 288, 107578. <https://doi.org/10.1016/j.quascirev.2022.107578>
- 847 Nalbant, J., Schneider, L., Hamilton, R., Connor, S., Biester, H., Stuart-Williams, H., Bergal-Kuvikas, O.,
848 Jacobsen, G., Stevenson, J., 2023. Fire, volcanism and climate change: the main factors controlling
849 mercury (Hg) accumulation rates in Tropical Lake Lantoa, Sulawesi, Indonesia (~16,500–540 cal yr BP).
850 *Frontiers in Environmental Chemistry* 4, 1241176. <https://doi.org/10.3389/fenvc.2023.1241176>
- 851 Nicholson, S.E., 2013. The West African Sahel: A Review of Recent Studies on the Rainfall Regime and Its
852 Interannual Variability. *ISRN Meteorology* 2013, 1–32. <https://doi.org/10.1155/2013/453521>
- 853 Obrist, D., Kirk, J.L., Zhang, L., Sunderland, E.M., Jiskra, M., Selin, N.E., 2018. A review of global environmental
854 mercury processes in response to human and natural perturbations: Changes of emissions, climate, and
855 land use. *Ambio* 47, 116–140. <https://doi.org/10.1007/s13280-017-1004-9>
- 856 Outridge, P.M., Stern, G.A., Hamilton, P.B., Sanei, H., 2019. Algal scavenging of mercury in preindustrial Arctic
857 lakes. *Limnology & Oceanography* 64, 1558–1571. <https://doi.org/10.1002/lno.11135>
- 858 Outridge, Sanei, H., Stern, Hamilton, Goodarzi, F., 2007. Evidence for Control of Mercury Accumulation Rates in
859 Canadian High Arctic Lake Sediments by Variations of Aquatic Primary Productivity. *Environmental*
860 *Science & Technology* 41, 5259–5265. <https://doi.org/10.1021/es070408x>
- 861 Paine, A.R., Fendley, I.M., Frieling, J., Mather, T.A., Lacey, J.H., Wagner, B., Robinson, S.A., Pyle, D.M.,
862 Francke, A., Them II, T.R., Panagiotopoulos, K., 2024. Mercury records covering the past 90 000 years
863 from lakes Prespa and Ohrid, SE Europe. *Biogeosciences* 21, 531–556. <https://doi.org/10.5194/bg-21-531-2024>
- 864
- 865 Pan, J., Zhong, W., Wei, Z., Ouyang, J., Shang, S., Ye, S., Chen, Y., Xue, J., Tang, X., 2020. A 15,400-year
866 record of natural and anthropogenic input of mercury (Hg) in a sub-alpine lacustrine sediment
867 succession from the western Nanling Mountains, South China. *Environmental Science and Pollution*
868 *Research* 27, 20478–20489. <https://doi.org/10.1007/s11356-020-08421-z>
- 869 Pausata, F.S.R., Gaetani, M., Messori, G., Berg, A., Maia de Souza, D., Sage, R.F., deMenocal, P.B., 2020. The
870 Greening of the Sahara: Past Changes and Future Implications. *One Earth* 2, 235–250.
871 <https://doi.org/10.1016/j.oneear.2020.03.002>
- 872 Peck, J.A., Green, R.R., Shanahan, T., King, J.W., Overpeck, J.T., Scholz, C.A., 2004. A magnetic mineral
873 record of Late Quaternary tropical climate variability from Lake Bosumtwi, Ghana. *Palaeoecology*,
874 *Palaeoecology* 215, 37–57. <https://doi.org/10.1016/j.palaeo.2004.08.003>



- 875 Pérez-Rodríguez, M., Margalef, O., Corella, J.P., Saiz-Lopez, A., Pla-Rabes, S., Giral, S., Cortizas, A.M., 2018.
876 The role of climate: 71 ka of atmospheric mercury deposition in the southern hemisphere recorded by
877 Rano Aroi Mire, Easter Island (Chile). *Geosciences (Switzerland)* 8.
878 <https://doi.org/10.3390/geosciences8100374>
- 879 Pilla, R.M., Williamson, C.E., Adamovich, B.V., Adrian, R., Anneville, O., Chandra, S., Colom-Montero, W.,
880 Devlin, S.P., Dix, M.A., Dokulil, M.T., Gaiser, E.E., Girdner, S.F., Hambright, K.D., Hamilton, D.P.,
881 Havens, K., Hessen, D.O., Higgins, S.N., Huttula, T.H., Huuskonen, H., Isles, P.D.F., Joehnk, K.D.,
882 Jones, I.D., Keller, W.B., Knoll, L.B., Korhonen, J., Kraemer, B.M., Leavitt, P.R., Lepori, F., Luger, M.S.,
883 Maberly, S.C., Melack, J.M., Melles, S.J., Müller-Navarra, D.C., Pierson, D.C., Pislegina, H.V., Plisnier,
884 P.-D., Richardson, D.C., Rimmer, A., Rogora, M., Rusak, J.A., Sadro, S., Salmaso, N., Saros, J.E.,
885 Saulnier-Talbot, É., Schindler, D.E., Schmid, M., Shimaraeva, S.V., Silow, E.A., Sitoki, L.M.,
886 Sommaruga, R., Straile, D., Strock, K.E., Thiery, W., Timofeyev, M.A., Verburg, P., Vinebrooke, R.D.,
887 Weyhenmeyer, G.A., Zadereev, E., 2020. Deeper waters are changing less consistently than surface
888 waters in a global analysis of 102 lakes. *Scientific Reports* 10, 20514. [https://doi.org/10.1038/s41598-](https://doi.org/10.1038/s41598-020-76873-x)
889 [020-76873-x](https://doi.org/10.1038/s41598-020-76873-x)
- 890 Pompeani, D.P., Cooke, C.A., Abbott, M.B., Drevnick, P.E., 2018. Climate, Fire, and Vegetation Mediate Mercury
891 Delivery to Midlatitude Lakes over the Holocene. *Environmental Science and Technology* 52, 8157–
892 8164. <https://doi.org/10.1021/acs.est.8b01523>
- 893 Ravichandran, M., 2004. Interactions between mercury and dissolved organic matter - A review. *Chemosphere*
894 55, 319–331. <https://doi.org/10.1016/j.chemosphere.2003.11.011>
- 895 Russell, J., Talbot, M.R., Haskell, B.J., 2003. Mid-holocene climate change in Lake Bosumtwi, Ghana.
896 *Quaternary Research* 60, 133–141. [https://doi.org/10.1016/S0033-5894\(03\)00065-6](https://doi.org/10.1016/S0033-5894(03)00065-6)
- 897 Sanei, H., Grasby, S., Beauchamp, B., 2012. Latest Permian mercury anomalies. *Geology* 40, 63–66.
- 898 Schneider, L., Cooke, C.A., Stansell, N.D., Haberle, S.G., 2020. Effects of climate variability on mercury
899 deposition during the Older Dryas and Younger Dryas in the Venezuelan Andes. *Journal of*
900 *Paleolimnology* 63, 211–224. <https://doi.org/10.1007/s10933-020-00111-7>
- 901 Schneider, L., Fisher, J.A., Diéguez, M.C., Fostier, A.-H., Guimaraes, J.R.D., Leaner, J.J., Mason, R., 2023. A
902 synthesis of mercury research in the Southern Hemisphere, part 1: Natural processes. *Ambio* 52, 897–
903 917. <https://doi.org/10.1007/s13280-023-01832-5>
- 904 Scholz, C.A., Johnson, T.C., Cohen, A.S., King, J.W., Peck, J.A., Overpeck, J.T., Talbot, M.R., Brown, E.T.,
905 Kalindekaf, L., Amoako, P.Y.O., Lyons, R.P., Shanahan, T.M., Castañeda, I.S., Heil, C.W., Forman,
906 S.L., McHargue, L.R., Beuning, K.R., Gomez, J., Pierson, J., 2007. East African megadroughts between
907 135 and 75 thousand years ago and bearing on early modern human origins. *PNAS USA* 104, 16416–
908 16421. <https://doi.org/10.1073/pnas.0703874104>
- 909 Schultze, M., Boehrer, B., Wendt-Potthoff, K., Katsev, S., Brown, E.T., 2017. Chemical Setting and
910 Biogeochemical Reactions in Meromictic Lakes, in: *Ecology of Meromictic Lakes*. Springer, pp. 35–61.
- 911 Schütze, M., Gatz, P., Giffedder, B., Biester, H., 2021. Why productive lakes are larger mercury sedimentary
912 sinks than oligotrophic brown water lakes. *Limnology & Oceanography* 66, 1316–1332.
913 <https://doi.org/10.1002/lno.11684>
- 914 Schütze, M., Tserendorj, G., Pérez-Rodríguez, M., Rösch, M., Biester, H., 2018. Prediction of Holocene mercury
915 accumulation trends by combining palynological and geochemical records of lake sediments (Black
916 Forest, Germany). *Geosciences (Switzerland)* 8. <https://doi.org/10.3390/geosciences8100358>
- 917 Sebag, D., Garcin, Y., Adatte, T., Deschamps, P., Ménot, G., Verrecchia, E.P., 2018. Correction for the siderite
918 effect on Rock-Eval parameters: Application to the sediments of Lake Barombi (southwest Cameroon).
919 *Organic Geochemistry* 123, 126–135. <https://doi.org/10.1016/j.orggeochem.2018.05.010>
- 920 Segato, D., Saiz-Lopez, A., Mahajan, A.S., Wang, F., Corella, J.P., Cuevas, C.A., Erhardt, T., Jensen, C.M.,
921 Zeppenfeld, C., Kjær, H.A., Turetta, C., Cairns, W.R.L., Barbante, C., Spolaor, A., 2023. Arctic mercury
922 flux increased through the Last Glacial Termination with a warming climate. *Nature Geoscience* 16,
923 439–445. <https://doi.org/10.1038/s41561-023-01172-9>
- 924 Selin, N.E., 2009. Global biogeochemical cycling of mercury: a review. *Annual Review of Environmental*
925 *Resources* 34, 43–63.
- 926 Shanahan, T.M., Beck, J.W., Overpeck, J.T., McKay, N.P., Pigati, J.S., Peck, J.A., Scholz, C.A., Heil, C.W., King,
927 J., 2012. Late Quaternary sedimentological and climate changes at Lake Bosumtwi Ghana: New
928 constraints from laminae analysis and radiocarbon age modeling. *Palaeogeography, Palaeoclimatology,*
929 *Palaeoecology* 361–362, 49–60. <https://doi.org/10.1016/j.palaeo.2012.08.001>
- 930 Shanahan, T.M., McKay, N.P., Hughen, K.A., Overpeck, J.T., Otto-Bliesner, B., Heil, C.W., King, J., Scholz, C.A.,
931 Peck, J., 2015. The time-transgressive termination of the African humid period. *Nature Geoscience* 8,
932 140–144. <https://doi.org/10.1038/ngeo2329>
- 933 Shanahan, T.M., Overpeck, J.T., Anchukaitis, K.J., Beck, J.W., Cole, J.E., Dettman, D.L., Peck, J.A., Scholz,
934 C.A., King, J.W., 2009. Atlantic forcing of persistent drought in West Africa. *Science* 324, 377–380.
935 <https://doi.org/10.1126/science.1166352>
- 936 Shanahan, T.M., Overpeck, J.T., Beck, J.W., Wheeler, C.W., Peck, J.A., King, J.W., Scholz, C.A., 2008a. The
937 formation of biogeochemical laminations in Lake Bosumtwi, Ghana, and their usefulness as indicators of
938 past environmental changes. *Journal of Paleolimnology* 40, 339–355. [https://doi.org/10.1007/s10933-](https://doi.org/10.1007/s10933-007-9164-4)
939 [007-9164-4](https://doi.org/10.1007/s10933-007-9164-4)



- 940 Shanahan, T.M., Overpeck, J.T., Scholz, C.A., Beck, J.W., Peck, J., King, J.W., 2008b. Abrupt changes in the
941 water balance of tropical West Africa during the late Quaternary. *Journal of Geophysical Research* 113,
942 D12108. <https://doi.org/10.1029/2007JD009320>
- 943 Shanahan, T.M., Overpeck, J.T., Sharp, W.E., Scholz, C.A., Arko, J.A., 2007. Simulating the response of a
944 closed-basin lake to recent climate changes in tropical West Africa (Lake Bosumtwi, Ghana).
945 *Hydrological Processes* 21, 1678–1691. <https://doi.org/10.1002/hyp.6359>
- 946 Shanahan, T.M., Overpeck, J.T., Wheeler, C.W., Beck, J.W., Pigati, J.S., Talbot, M.R., Scholz, C.A., Peck, J.,
947 King, J.W., 2006. Paleoclimatic variations in West Africa from a record of late Pleistocene and Holocene
948 lake level stands of Lake Bosumtwi, Ghana. *Palaeogeography, Palaeoclimatology, Palaeoecology* 242,
949 287–302. <https://doi.org/10.1016/j.palaeo.2006.06.007>
- 950 Shanahan, T.M., Peck, J.A., McKay, N., Heil, C.W., King, J., Forman, S.L., Hoffmann, D.L., Richards, D.A.,
951 Overpeck, J.T., Scholz, C., 2013. Age models for long lacustrine sediment records using multiple dating
952 approaches - An example from Lake Bosumtwi, Ghana. *Quaternary Geochronology* 15, 47–60.
953 <https://doi.org/10.1016/j.quageo.2012.12.001>
- 954 Shen, J., Feng, Q., Algeo, T.J., Liu, Jinling, Zhou, C., Wei, W., Liu, Jiangsi, Them, T.R., Gill, B.C., Chen, J., 2020.
955 Sedimentary host phases of mercury (Hg) and implications for use of Hg as a volcanic proxy. *Earth and*
956 *Planetary Science Letters* 543, 116333. <https://doi.org/10.1016/j.epsl.2020.116333>
- 957 Skonieczny, C., McGee, D., Winckler, G., Bory, A., Bradtmiller, L.I., Kinsley, C.W., Polissar, P.J., De Pol-Holz, R.,
958 Rossignol, L., Malaizé, B., 2019. Monsoon-driven Saharan dust variability over the past 240,000 years.
959 *Science Advances* 5, 1–9. <https://doi.org/10.1126/sciadv.aav1887>
- 960 Soerensen, A.L., Mason, R.P., Balcom, P.H., Jacob, D.J., Zhang, Y., Kuss, J., Sunderland, E.M., 2014.
961 Elemental Mercury Concentrations and Fluxes in the Tropical Atmosphere and Ocean. *Environmental*
962 *Science & Technology* 48, 11312–11319. <https://doi.org/10.1021/es503109p>
- 963 Sprovieri, F., Pirrone, N., Bencardino, M., D'Amore, F., Angot, H., Barbante, C., Brunke, E.-G., Arcega-Cabrera,
964 F., Cairns, W., Comero, S., Diéguez, M. del C., Dommergue, A., Ebinghaus, R., Feng, X.B., Fu, X.,
965 Garcia, P.E., Gawlik, B.M., Hageström, U., Hansson, K., Horvat, M., Kotnik, J., Labuschagne, C.,
966 Magand, O., Martin, L., Mashyanov, N., Mkololo, T., Munthe, J., Obolkin, V., Ramirez Islas, M., Sena,
967 F., Somerset, V., Spandow, P., Vardè, M., Walters, C., Wängberg, I., Weigelt, A., Yang, X., Zhang, H.,
968 2017. Five-year records of mercury wet deposition flux at GMOS sites in the Northern and Southern
969 hemispheres. *Atmospheric Chemistry & Physics* 17, 2689–2708. [https://doi.org/10.5194/acp-17-2689-](https://doi.org/10.5194/acp-17-2689-2017)
970 2017
- 971 Sprovieri, F., Pirrone, N., Ebinghaus, R., Kock, H., Dommergue, A., 2010. A review of worldwide atmospheric
972 mercury measurements. *Atmospheric Chemistry and Physics* 10, 8245–8265.
973 <https://doi.org/10.5194/acp-10-8245-2010>
- 974 Swart, P.K., 2015. The geochemistry of carbonate diagenesis: The past, present and future. *Sedimentology* 62,
975 1233–1304. <https://doi.org/10.1111/sed.12205>
- 976 Talbot, M.R., Johannessen, T., 1992. A high resolution palaeoclimatic record for the last 27,500 years in tropical
977 West Africa from the carbon and nitrogen isotopic composition of lacustrine organic matter. *Earth and*
978 *Planetary Science Letters* 110, 23–37. [https://doi.org/10.1016/0012-821X\(92\)90036-U](https://doi.org/10.1016/0012-821X(92)90036-U)
- 979 Them, T.R., Jagoe, C.H., Caruthers, A.H., Gill, B.C., Grasby, S.E., Gröcke, D.R., Yin, R., Owens, J.D., 2019.
980 Terrestrial sources as the primary delivery mechanism of mercury to the oceans across the Toarcian
981 Oceanic Anoxic Event (Early Jurassic). *Earth and Planetary Science Letters* 507, 62–72.
982 <https://doi.org/10.1016/j.epsl.2018.11.029>
- 983 Tisserand, D., Guédron, S., Viollier, E., Jézéquel, D., Rigaud, S., Campillo, S., Sarret, G., Charlet, L., Cossa, D.,
984 2022. Mercury, organic matter, iron, and sulfur co-cycling in a ferruginous meromictic lake. *Applied*
985 *Geochemistry* 146, 105463. <https://doi.org/10.1016/j.apgeochem.2022.105463>
- 986 Tjallingii, R., Claussen, M., Stuut, J.-B.W., Fohlmeister, J., Jahn, A., Bickert, T., Lamy, F., Röhl, U., 2008.
987 Coherent high- and low-latitude control of the northwest African hydrological balance. *Nature*
988 *Geoscience* 1, 670–675. <https://doi.org/10.1038/ngeo289>
- 989 Trauth, M.H., Asrat, A., Berner, N., Bibi, F., Foerster, V., Grove, M., Kaboth-Bahr, S., Maslin, M.A., Mudelsee, M.,
990 Schäbitz, F., 2021. Northern Hemisphere Glaciation, African climate and human evolution. *Quaternary*
991 *Science Reviews* 268, 107095. <https://doi.org/10.1016/j.quascirev.2021.107095>
- 992 Tribouillard, N., Algeo, T.J., Lyons, T., Riboulleau, A., 2006. Trace metals as paleoredox and paleoproductivity
993 proxies: An update. *Chemical Geology* 232, 12–32. <https://doi.org/10.1016/j.chemgeo.2006.02.012>
- 994 Turner, B.F., Gardner, L.R., Sharp, W.E., 1996. The hydrology of lake Bosumtwi, a climate-sensitive lake in
995 Ghana, West Africa. *Journal of Hydrology* 183, 243–261. [https://doi.org/10.1016/0022-1694\(95\)02982-6](https://doi.org/10.1016/0022-1694(95)02982-6)
- 996 United Nations Environment Programme, 2018. *Global Mercury Assessment*, United Nations.
- 997 Vinušková, O., Jandová, K., Frouz, J., 2019. Improved method for removing siderite by *in situ* acidification
998 before elemental and isotope analysis of soil organic carbon. *Journal of Plant Nutrition and Soil Science*
999 182, 82–91. <https://doi.org/10.1002/jpln.201800164>
- 1000 Weldeab, S., Lea, D.W., Schneider, R.R., Andersen, N., 2007. 155,000 Years of West African Monsoon and
1001 Ocean Thermal Evolution. *Science* 316, 1303–1307. <https://doi.org/10.1126/science.1140461>
- 1002 White, F. (Frank), 1983. *The vegetation of Africa: a descriptive memoir to accompany the*
1003 *Unesco/AETFAT/UNSO vegetation map of Africa, Natural resources research ; 20*. Unesco, Paris.
- 1004 Woolway, R.I., Kraemer, B.M., Lenters, J.D., Merchant, C.J., O'Reilly, C.M., Sharma, S., 2020. Global lake
1005 responses to climate change. *Nature Reviews Earth and Environment* 1, 388–403.
1006 <https://doi.org/10.1038/s43017-020-0067-5>



- 1007 Zaferani, S., Biester, H., 2021. Mercury Accumulation in Marine Sediments – A Comparison of an Upwelling Area
1008 and Two Large River Mouths. *Frontiers in Marine Science* 8, 732720.
1009 <https://doi.org/10.3389/fmars.2021.732720>
1010 Zolitschka, B., Francus, P., Ojala, A.E.K., Schimmelmann, A., 2015. Varves in lake sediments - a review.
1011 *Quaternary Science Reviews* 117, 1–41.
1012 Zou, J., Chang, Y.P., Zhu, A., Chen, M.T., Kandasamy, S., Yang, H., Cui, J., Yu, P.S., Shi, X., 2021. Sedimentary
1013 mercury and antimony revealed orbital-scale dynamics of the Kuroshio Current. *Quaternary Science*
1014 *Reviews* 265, 107051. <https://doi.org/10.1016/j.quascirev.2021.107051>
1015